The University of Kansas
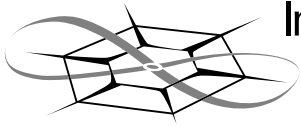
Information and Telecommunication Technology Center

Technical Report

Model Based Signal Processing Algorithm for MIDP GPR

Visweswaran Srinivasamurthy,
Dr. Muhammad Dawood, and Dr. Sivaprasad Gogineni

June 2005

ITTC-FY2005-TR-32060-01

ACKNOWLEDGMENTS

Abstract

The use of Ground-penetrating Radar (GPR) for geological exploration, among other applications, is gaining widespread acceptance. Specifically, radars are being used to characterize multilayered media. To characterize surface and subsurface layers from recorded radar data, we are faced with the problem of detecting weak signals buried in the sidelobes of stronger reflections. Conventional windowing techniques can be used to reduce sidelobes; however, they attenuate the lower frequencies that contain most of the information about the deeper structure of the multi-layered target. The primary objective of this research is to develop a signal processing algorithm to minimize range sidelobes for the enhancement of subsurface features. We also wish to extend the algorithm to characterize the constituents of the subsurface layers in terms of an equivalent electrical parameter called Permittivity.

The GPR data are corrupted with noise, scattering components and losses due to the random nature of the underlying subsurface and due to the attenuation of high frequency components through subsurface layers. It has often been shown that signal processing schemes that incorporate the underlying physical phenomena that generated the measured signal (also called the *Model Based Approach*) offer better performance in terms of a minimum variance estimate. To this end, we undertook the study on model based techniques for the purpose of signal enhancement and data inversion. Specifically, we analyzed the performance of Regression based techniques (such as the Gauss Newton method) and Spectral Estimation techniques (MUSIC) to achieve our objectives. In this work, we present the results of our study through simulations and tests conducted on

actual radar data. Finally, we have also developed a Graphical User Interface for the inversion algorithm using MATLAB, the details of which have also been explained in this report.

TABLE OF CONTENTS

LIST OF FIGURES

LIST OF TABLES

Chapter 1

Introduction

1.1 Motivation

NASA has structured the Mars Exploration Program (MEP) [1] for a series of highly ambitious missions to Mars over the next decade. The MEP plans to send several landers/orbiters to Mars to achieve some of the following objectives:

1. Increase the understanding of the availability and amount of water on Mars.

2. Identify the composition of rocks and soils within the Martian surface.

3. Determine the nature of geological processes from surface morphology.

4. Improve understanding of the Mars climate by analysis of *in-situ* materials.

In order to achieve these objectives, we need intelligent remote sensing techniques. In this regard, NASA designed the Mars Instrument Development Project (MIDP) to develop instruments that can be deployed on the Martian surface to gather geological data.

1.2 Radars in Remote Sensing

The use of radars in remote sensing of the environment is well known [2]. The original purpose of radars was to detect the presence of targets. However, with advancements in technology, radars are now being used to characterize the targets based on their constituents. This is commonly known as the *EM (Electro-Magnetic) Inversion Problem* in Radar - where the goal is to estimate the composition of materials using data collected by a radar. A Ground Penetrating Radar (GPR) uses electromagnetic waves

(typically in the frequency range of 10 MHz to 1000 MHz) to extract information about targets.

In the field of geology, we come across a fundamental term called stratigraphy, which is defined as the physical distribution of rocks and soils beneath the target surface under observation. From a radar point of view, stratigraphy refers to the distribution of the electrical properties (permittivity and permeability) of materials.

The EM wave radiated from a transmitter antenna travels through different media (at a velocity governed by the electrical properties of the material), and if it encounters a boundary with differing electrical properties, a part of the wave energy is reflected or scattered back to the surface, while part of the energy continues to travel downward. The amplitude of the reflected signal depends on the dielectric contrast between successive media. The radar receiver collects the composite return signal consisting of several returns from various layers of different dielectric constants.

NASA, in association with the Italian Space Agency, has developed MARSIS (Mars Advanced Radar for Subsurface and Ionosphere Sounding) to be tested on the Martian surface [3]. This instrument will perform sub-surface sounding of the Martian crust. The collected data will then be processed to characterize subsurface features. More specifically, scientists are interested to know if water exists on Mars. This forms the primary motivating factor for this research, which addresses the two-fold objectives of:

1. Enhancing the features of the radar signal (to detect subsurface layers); and

2. Inverse permittivity profiling: Estimating the permittivity (dielectric constant) profile of a multi-layered media using GPR recorded data.

This necessitates the development of a signal processing scheme that can estimate the unknown electrical parameters from a composite signal seen by the radar. From a mathematical point of view, this problem is called *Parameter Estimation.* Figure 1-1 illustrates the problem statement pictorially.
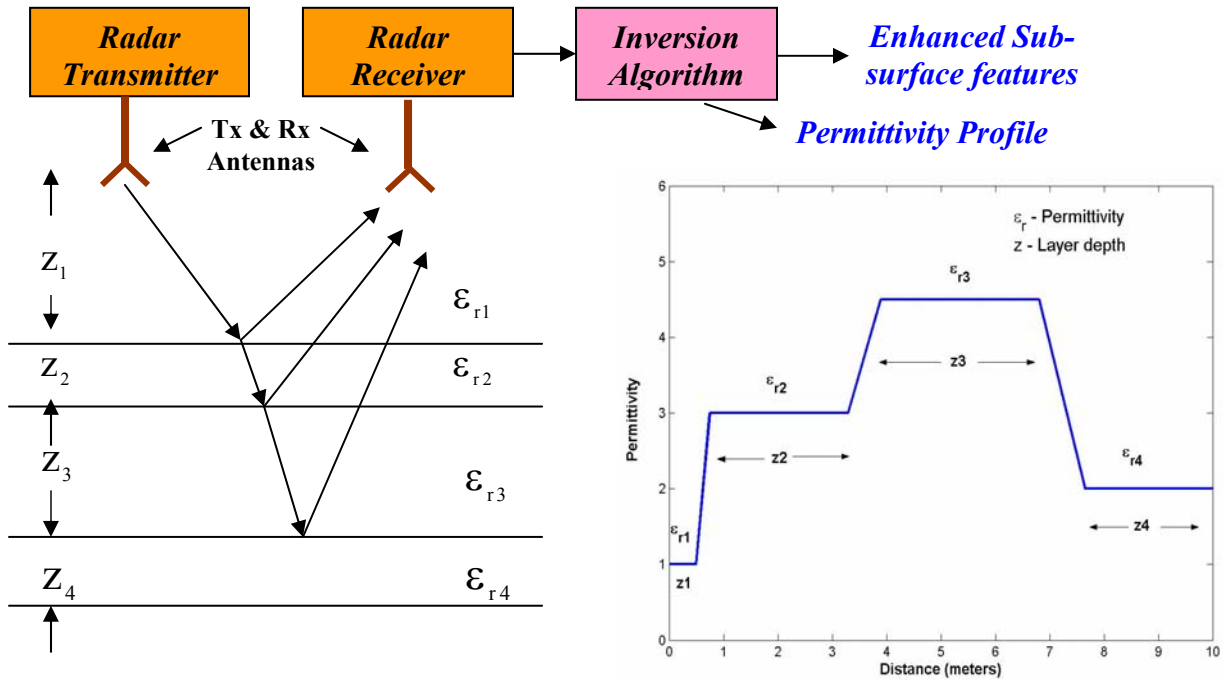
Figure 1-1 EM phenomenon for a Multilayered target case; A typical permittivity profile

There are many problems in the analysis of radar data. If the radar measures only the reflections from layers with contrasts in permittivity, then it is easy to estimate the unknown parameters. However, there are several other factors, such as scattering, attenuation and additive noise, that corrupt the return; hence, this is a non-linear problem, and without some prior knowledge of the geo-physical structure, it is hard to find a solution to this problem.

Conventionally, the Fourier (or Inverse Fourier) Transform algorithm is applied to the received signal (in frequency domain/time domain) and is converted into the range

profile. This composite return may contain weaker signals from deeper layers. The major disadvantage of using Fourier transform techniques is the range sidelobes, which can mask weaker reflections from deeper layers [4]. Normally, windowing functions can help reduce the side lobes of strong reflections. However, the use of these windowing functions will attenuate the lower frequencies that contain most of the information about the deeper structure of the surface. Hence, it is necessary to develop a signal processing algorithm to minimize the range side lobes for enhancement of sub-surface features and then reconstruct the permittivity profile.

1.3 The Model-Based Approach

Typically, model-based techniques attempt to estimate the unknown parameters by comparing the measured radar target signatures with a mathematical model such that it closely follows the underlying physical phenomenon. Figure 1-2 below depicts the model based approach to data inversion.
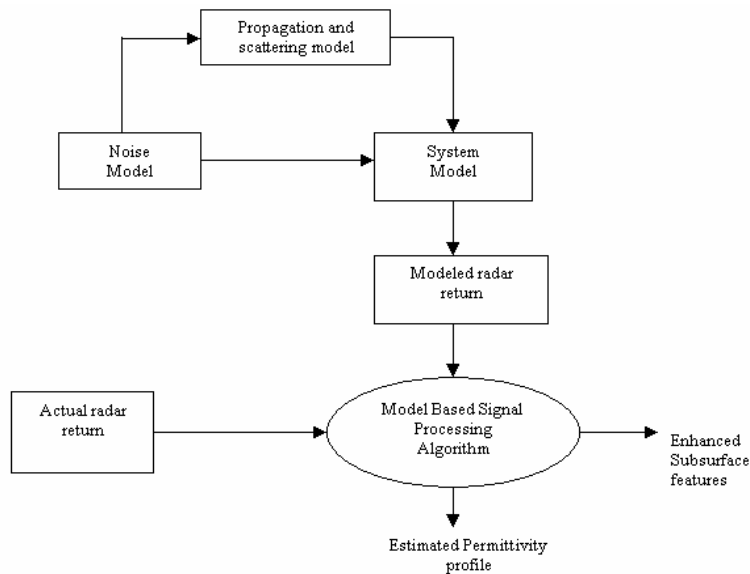
Figure 1-2 The model-based approach for data inversion

4

Broadly, Model Based Techniques fall under two categories – MMSE Minimization and Spectral Estimation. In the MMSE minimization approach, the unknown permittivity is estimated based on the principle of minimizing the mean square error between the measured and the modeled data. The Gauss Newton Method and Kalman Filter algorithm [5] are two well known algorithms in this category. In the spectral estimation approach, permittivity is estimated by first estimating unknown frequency components in the return signal spectrum and then estimating reflection coefficient amplitudes with a likelihood estimator. Well known spectral estimation algorithms are the Multiple Signal Classification (MUSIC) algorithm, Minimum norm algorithm and the Eigen vector algorithm. In all of these algorithms, it is necessary to have a good GPR response model (forward model) that relates model parameters to the underlying geophysical phenomenon.

In order to model a GPR response, there are a variety of simulation methods. For a basic first-order simulation, a simple convolution-based modeling technique is used. For more accurate results, the effects of scattering due to random surfaces and the three dimensional antenna beam pattern can be obtained using more advanced methods such as the Finite Difference Time Domain (FDTD) method, at the cost of complexity and computational time. In this research, we have considered the first method: the convolution-based approach.

1.4 Organization

This report is organized into six chapters. The objectives and principles behind this research are explained in detail in Chapter 2, while Chapter 3 addresses the problem

of enhancement of subsurface layers using FFT and a high resolution algorithm called MUSIC. In Chapter 4, we address the problem of inverse permittivity profiling. A few methods for data inversion are presented here. Chapter 5 describes the testing of the inversion algorithm on actual FMCW radar data collected during field experiments in Antarctica and Greenland. The algorithm was also tested in the sandbox facility of the Radar Systems and Remote Sensing Lab (RSL) of the University of Kansas. The results of this test are also presented. Chapter 6 describes the Graphical User Interface (GUI) developed for the model-based inversion. The concluding chapter summarizes our work and contains some recommendations for further research.

Chapter 2

The Problem Statement

Broadly, we are dealing with the study of a geophysical phenomenon - namely, the reflection of EM waves due to dielectric contrast between media. To address the objectives of this work, the overall problem has been broken down into four major steps [6].

1. *System parameterization:* This involves discovering the set of model parameters whose values completely characterize the system (phenomenon). For the problem at hand, this parameter which characterizes the geo-physical phenomenon is the permittivity of multi-layered media.

2. *Forward Modeling:* This step involves discovering the underlying physical phenomenon and deducing a mathematical relationship between the model parameters and actual observations. In this research we are dealing with the propagation and reflection of EM waves, which are dependent on the underlying permittivity profile.

3. *Enhancement of reflectivity profiles:* This forms the primary objective of our work where we apply suitable signal processing techniques to obtain high resolution reflectivity maps of the radar signal for analysis. This part is discussed in Chapter 3.

4. *Inverse Modeling:* This involves the use of the actual results of some measurements of the observable parameters to infer the actual values of the model parameters. This problem is addressed in Chapter 4.

2.1 Forward Modeling

In order to better analyze a geophysical phenomenon, the very phenomenon (system) may be modeled (simulated), if we can relate the parameters responsible for the phenomenon and the response of the system. In order to model the return signal from a multi-layered target, we first consider the propagation of EM waves through dielectric media and how they influence the return signal.

In modeling horizontally layered media, it is a common approach to consider plane wave approximation for EM propagation [7]. This means that it is assumed that the multiple layers are perfectly planar and that the antenna beam is like a pencil beam, as shown in Figure 2-1.
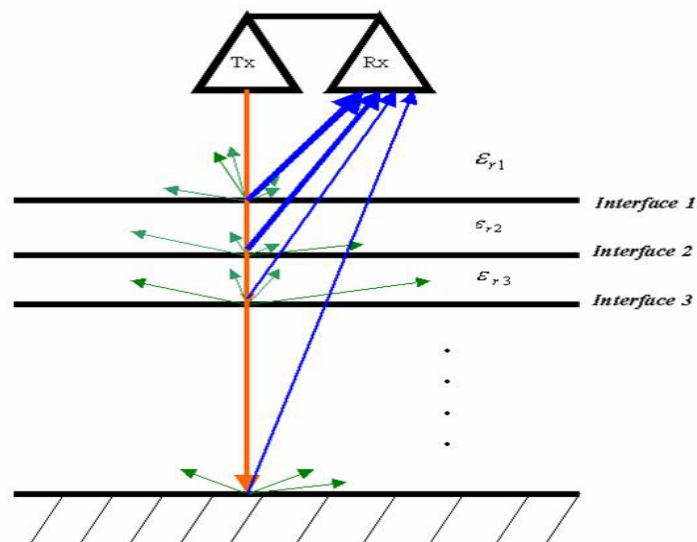
Figure 2-1 Multi-layered target with different dielectric boundaries

2.1.1 Permittivity

The underlying fundamental electrical parameter responsible for the reflection of EM waves is called Permittivity or the dielectric constant of the material. From an electromagnetics point of view, permittivity is a measure of how much a medium changes to absorb energy upon the influence of an electric field. For good dielectric materials, permittivity is a real quantity and is determined by the displacement current flowing through it. In the case of a lossy medium, conduction currents also flow through the material, and we define a complex value for permittivity as [7] :

$$\varepsilon = \varepsilon^{'} - j\varepsilon^{''}$$

(2.1)

where $\varepsilon^{'}$ is the real part of permittivity and it represnts the capacity of the medium to store EM energy. The imaginary part of permittivity, $\varepsilon^{''}$ represents the EM energy losses [7] (due to absorptive properties of the medium). In general, permittivity is a function of frequency, but for the purposes of simplicity, we will assume a *frequency-independent* situation for our problem.

Every material on earth has a unique value of permittivity. If not for the concept of permittivity, we wouldn't be able to distinguish between ice, water and snow, which are just different forms of the same material. Ice has a permittivity of around 3.14, it is around 80 for water, and for snow, it can vary depending on its density and moisture content. Hence, the underlying permittivity is responsible for each of these materials interacting in a different way with the same incident EM wave. As will be seen in the next chapter, radars exploit this phenomenon and are successfully being used in remote sensing to characterize materials.

2.2 Wave Propagation Phenomena

When an EM wave propagating down strikes layers of differing dielectric constants, the following phenomena occur:

2.2.1 Reflection & Transmission

Whenever an EM wave encounters a dielectric interface, a part of the incident signal is reflected back to the source and a part of it propagates into the layer. The reflected signal amplitude is proportional to the reflection coefficient at the dielectric interface defined as the ratio of the positive directed field divided by the negative directed field or alternatively, the ratio of the reflected wave divided by the incident wave. In mathematical terms, the reflection coefficient denoted by Γ_k is defined as [7] :

$$\Gamma_k = \left(\sqrt{\varepsilon_{k+1}} - \sqrt{\varepsilon_k} \right) \Big/ \left(\sqrt{\varepsilon_{k+1}} + \sqrt{\varepsilon_k} \right) \tag{2.2}$$

where ε_k is the permittivity of layer k and ε_{k+1} represents the permittivity of the next layer. The portion of the EM wave transmitted is quantified by the Transmission coefficient (T_k) and is mathematically related to permittiviy as :

$$T_k = \sqrt{4\sqrt{\varepsilon_k \varepsilon_{k+1}} \Big/ \left[\sqrt{\varepsilon_{k+1}} + \sqrt{\varepsilon_k} \right]^2} \tag{2.3}$$

Hence, a positive value of reflection coefficient indicates an increasing dielectric profile and a negative value indicates a decreasing profile at the interface.

2.2.2 Attenuation

As seen earlier, EM energy returns to the radar because of reflection. However, part of the EM energy that is not reflected propagates further into the medium and can get attenuated. Given below are some of the phenomena that may attenuate an EM signal.

2.2.2.1 Scattering

Scattering is a phenomenon that occurs due to the interaction of EM waves with irregular (rough) surfaces. Hence we have the concept of *surface scattering*. The second type of scattering is called *volume scattering*. Volume scattering occurs because the multiple target layers are not homogenous. Rather, the layers are a mixture of particles suspended in a background medium. In our analysis, the effects of attenuation due to scattering have been neglected for simplicity.

2.2.2.2 Absorption

Certain materials have the property of absorbing EM radiation when incident on them. Hence, the EM wave is attenuated. From an electrical point of view, we normally include an "Absorption coefficient" to model the attenuation due to absorption [8]. This coefficient depends on the particle size, wetness percentage, type of background material, etc.

2.2.2.3 Spreading

When a power of P_t is transmitted by an antenna having gain G_t, the power at a distance **R** from the antenna is given by

$$P_r = P_t G_t \left(\frac{1}{4\pi R^2} \right) \tag{2.4}$$

Here, the term in brackets denotes the free space spreading loss due to the antenna beam pattern. Hence, for a two way distance of **2R**, there is a loss of $\left(2\middle/4\pi R^2\right)$ due to spreading.

2.2.3 Modeling Target Response

If all of the above factors can be accurately determined, we can essentially construct the radar return using simulations. This is called the Forward Modeling of Radar Signal. So far, we looked at various factors that can influence radar return and their mathematical interpretation. Now, we will look at combining all these factors to model the overall composite signal that reaches the radar receiver. Figure 2-2 below gives a simplified notion of the discussion thus far.
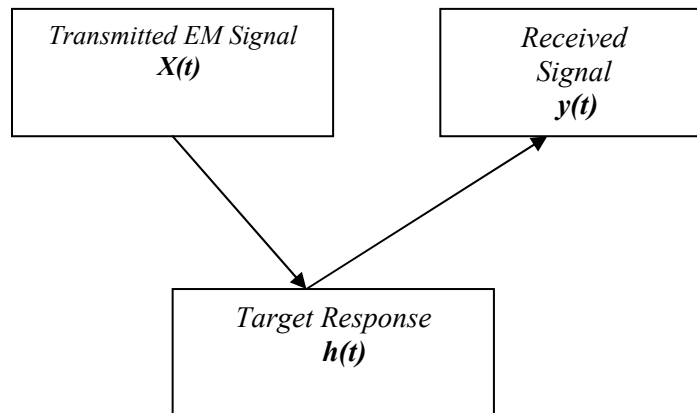
Figure 2-2 Block diagram of the forward modeling problem

The response of a system to an impulse is called the *impulse response* of the system. The impulse response of a multi-layered target can be modeled from its contributing parameters discussed above. In order to model the physical phenomenon, a widely accepted method is the *convolution-based* scheme based on one-dimensional modeling [4]. This means that, if we denote the transmitted signal as *x(t)* and the target response as *h(t)*, then the received radar signal is simply the convolution of *x(t)* and *h(t)*.

This is based on the assumption that the plane wave propagation or the ray propagation

model holds good to represent the phenomenon. Convolution in the time domain

corresponds to multiplication in the frequency domain. Hence, we can also write:

$$Y(f) = H(f) \cdot X(f) \qquad (2.5)$$

where each of these terms represents the transfer function of its corresponding impulse

response. A graphical illustration of the overall forward modeling problem [10] is

presented in figure 2-3.
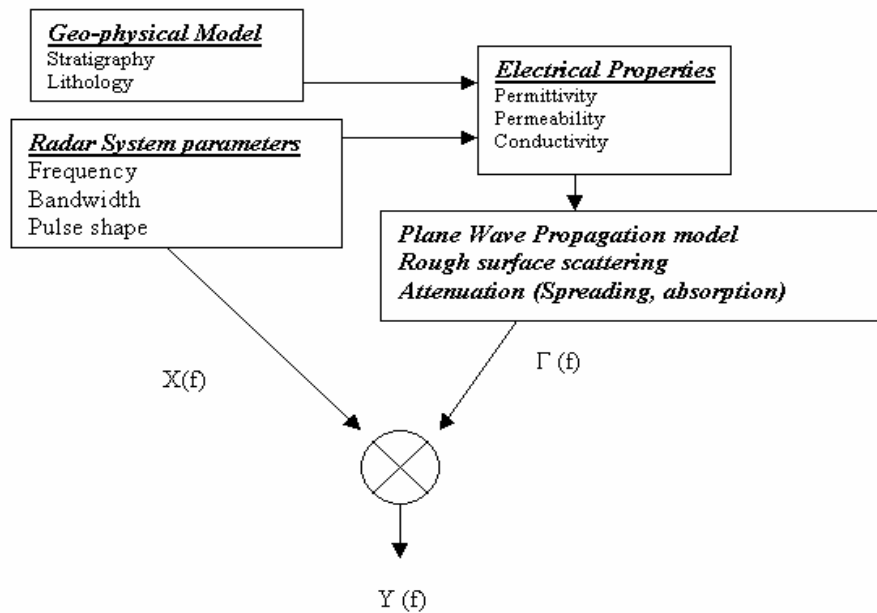
Figure 2-3 Simulation Flow chart

There are other advanced techniques for forward modeling, such as the Finite

Difference Time domain (FDTD) which takes into account phenomena such as multiple

reflections, interferences, geometrical spreading, ray focusing, phase shifts, etc., which

are ignored by the convolution model seen earlier [11]. However, these techniques

require a large computing time, complicating simple implementation. Hence, in this work we will focus on the convolution model for simplicity.

We now present simulations in MATLAB for a Frequency Modulated Continuous Wave (FMCW) radar to illustrate the concept of forward modeling. The first step is to model the return signal from an FMCW radar.

2.3 FMCW Radar Modeling

The FMCW radar transmits a frequency sweep, also called a chirp signal [12] (Figure 2-4). The reflected signal is basically an attenuated and frequency shifted version of the transmit signal.
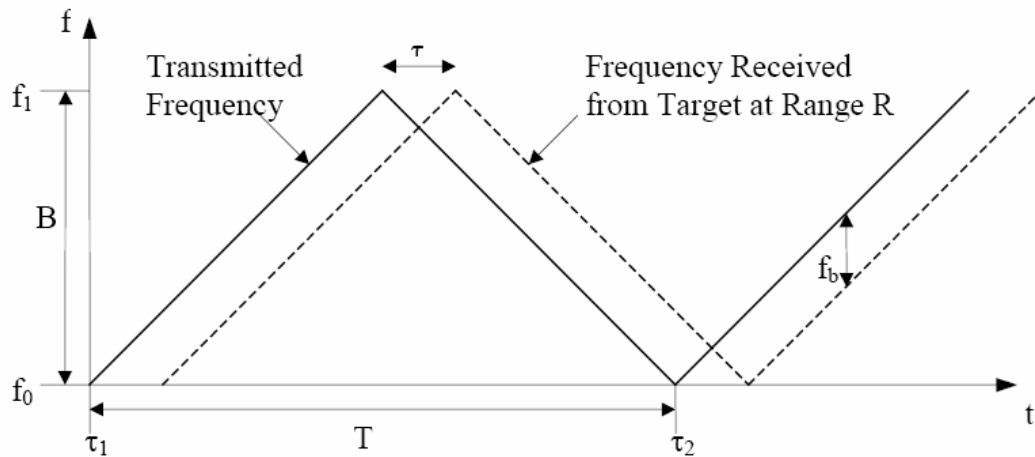
Figure 2-4 FMCW - Chirp Waveform

The composite reflected signal is mixed with a copy of the transmitted signal to determine the range of the target. The difference between the transmitted and the received signal is called the IF Signal or Beat Signal and the shift in received frequency is called the Beat Frequency, which is directly proportional to the range to the target. The instantaneous frequency of the transmit chirp is given by:

$$f(t) = f_0 + \alpha t \qquad (2.6)$$

where f_0 is the starting frequency of the chirp and α is called the chirp rate, defined as the ratio of bandwidth (**B**) to the sweep duration (**T**).

The received signal can be mathematically modeled from a simplified model of the FMCW radar as depicted in Figure 2-5.
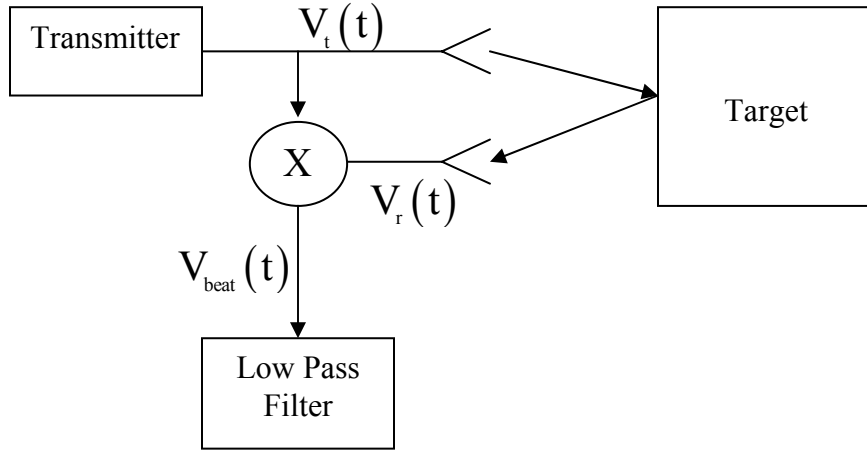
Figure 2-5 Simplified Model of an FMCW Radar

The signal at the output of the low pass filter may be derived for a multi-layered target as:

$$V_{beat}(\tau) = \sum_{k=0}^{L-1} A_k \Gamma_k \prod_{j=1}^{k-1} T_j \cos(2\pi\{f_0\tau_k + \alpha\tau_k(2t - \tau_k)\} + W \qquad (2.7)$$

where all terms carry the same meaning as discussed earlier. We account for system noise by modeling it by a Gaussian random variable (W).

The Fast Fourier Transform (FFT) algorithm is applied on the beat signal $V_{beat}(\tau)$ to obtain the frequency response of the target, which is also called the Range profile or a plot showing the variation of received amplitude as a function of target distance.
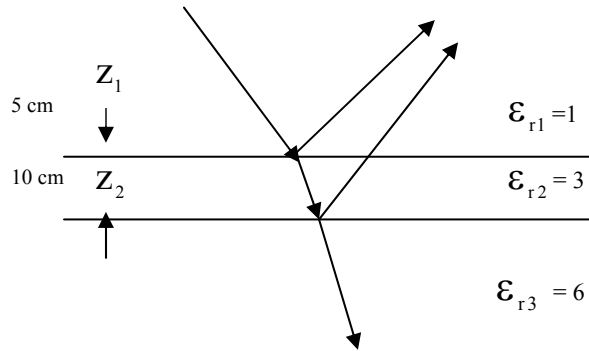
Figure 2-6 A Multilayered Profile

To demonstrate the modeling of an FMCW radar, let us assume a multilayered dielectric profile as depicted in Figure 2-6 shown above. Table 2-1 below shows the parameters considered for MATLAB simulation along with the geophysical profile vectors ε_r and **Z.**

Table 2-1 Radar parameters and geophysical parameters for FMCW radar modeling

Bandwidth	6 GHz
Start Frequency	2 GHz
Sweep time	10 ms
Chirp rate	300 GHz/s
Permittivity vector ε_r	[1 3 6]
Depth vector **Z** (cm)	[5 10]
Beat frequency vector $f_b = \dfrac{2RB}{Tc}$ (Hz)	[400 1785.6]

The beat frequencies corresponding to their respective distances are also indicated in the table above. Figure 2-7 below shows the range profile obtained by modeling the above profile. We can see peaks corresponding to beat frequencies 400 Hz and 1785.6 Hz, which are identical to the mathematically calculated beat frequencies.

16
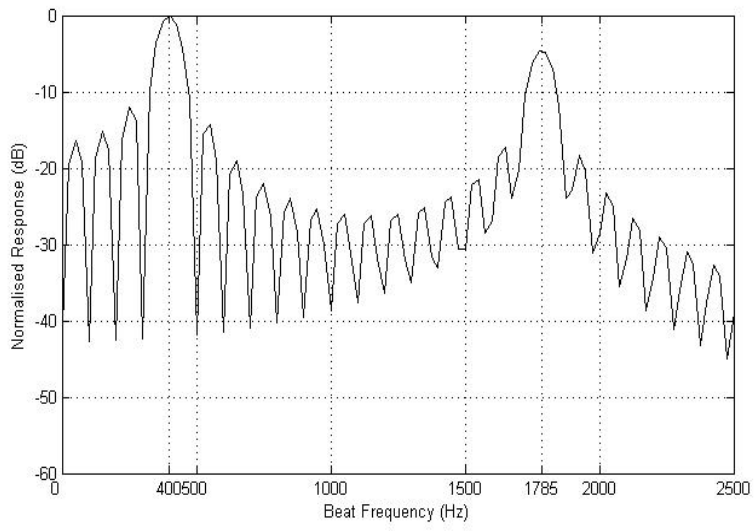
Figure 2-7 Range Profile obtained by taking IFFT

Chapter 3

Enhancement of sub-surface features

As seen in Chapter 2, the FFT on the return signal yields the signal spectrum (also called the range profile), which shows peaks occurring at their corresponding depths. However, Fourier-based techniques for spectral analysis have a fundamental limitation in that their resolution is strictly dependent on the bandwidth of operation of the radar system and hence, in the case of bandwidth-limited systems, FFTs offer very poor resolution, thus making it difficult to detect the presence of deeper subsurface layers. To illustrate this problem, we consider a 5-layer profile (Table 3-1)

Table 3-1 Five layer profile to demonstrate the problem of enhancement

Bandwidth	3 GHz
Start Frequency	2 GHz
Sweep time	10 ms
Permittivity vector ε_r	[1 5 4.5 3 3.7]
Depth vector $\mathbf{Z}$ (cm)	[50 7 20 30]
Range resolution	5 cm (free space)

Using the forward model of (2.7) with an SNR of 10 dB, the radar received signal was modeled in MATLAB and the range profile using the FFT is shown plotted in Figure 3-2 below.
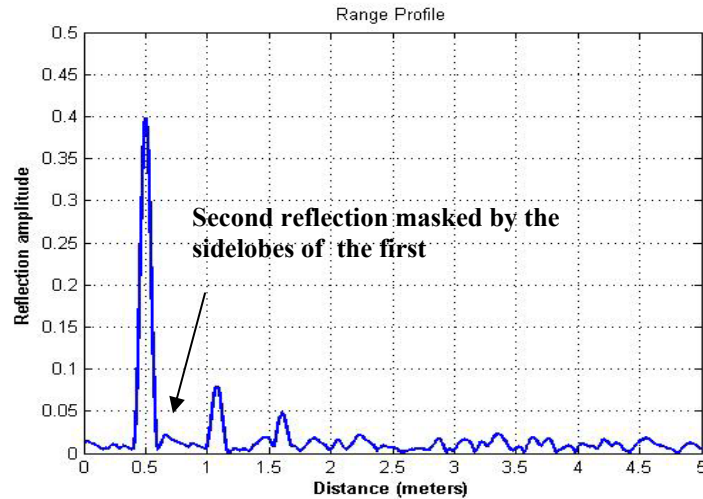
Figure 3-1 Range Profile of Table 1 plotted using FFT

It is seen that the dielectric contrast at the second interface results in a weak reflection and is buried under the sidelobes of the surface return, which is much stronger than the second reflection. Hence, target identification using the FFT is not a very effective method in the following cases:

1. Geophysical profiles with subtle variations in permittivity

2. Bandwidth limited (or comparatively small bandwidth) radar systems with poor resolution capabilities

Hence, we find the need for techniques with good resolution capability to obtain improved reflectivity profiles.

3.1 Parametric (Model - Based) Spectral Estimation

Parametric spectral estimation methods estimate unknown parameters from the given data by incorporating a model for the observed process into the estimation algorithm. It is for this reason that parametric methods promise significant improvement

in resolution of the frequency estimate and can be applied to the problem under consideration [13].

Commonly, for radar problems, a harmonic model is assumed since it is well known that radars measure a composite summation of sinusoids of different frequencies (depending on the distance traveled by the signal) embedded in noise. Schmidt [14] came up with a super-resolution frequency technique called MUSIC, which stands for **MU**ltiple **SI**gnal **C**lassification. This method is an extension of the Pisarenko Harmonic Decomposition method [15], which works on the principle that it is possible to estimate unknown sinusoidal components embedded in noise from the eigenvector corresponding to the minimum eigenvalue of the autocorrelation matrix by exploiting the orthogonality of signal subspace and the noise subspace. The first step in implementing MUSIC for high resolution frequency estimation is the development of a good model for the observed data. Typically, the radar received signal can be modeled as:

$$x(n) = \sum_{k=1}^{P} A_k \, e^{j \cdot f(\omega_k)} + w(n) \tag{3.1}$$

where $n = 1,2\ldots N\text{-}1$, with N being the number of samples of the observation, A_k denotes the signal amplitude from layer k modeled using (3), P represents the number of sinusoids in the signal $x(n)$, $w(n)$ denotes additive white Gaussian noise with mean zero and variance σ^2, and $f(\omega_k)$ denotes the term dependent on the unknown frequency variable and takes a functional relationship depending on the type of radar used. As seen in Section 2.3, for an FMCW radar, this function can be written in terms of time delays as

$$f(\tau_k) = f_0 \tau_k + \alpha \tau_k \left(2t - \tau_k\right) \tag{3.2}$$

For an FMCW radar, time delay and beat frequency are related as

$$\tau_k = \frac{\omega_k T}{2 \pi B} \qquad (3.3)$$

where T is the duration of the frequency sweep and B is the bandwidth of operation.

Hence we have an equivalent function in τ_k.

Once the signal model has been formulated, MUSIC uses the eigen structure of the correlation matrix of the measured data for spectrum estimation.

We write the signal autocorrelation function as

$$R_X = E\left[xx^H \right] \qquad (3.4)$$

where E [.] denotes the ensemble average. Since it is known that the received data is the sum of sinusoids embedded in noise (assumed to be uncorrelated with the signal), the data correlation matrix may be subdivided into two parts as

$$R_X = R_S + R_n \qquad (3.5)$$

where R_S is the autocorrelation matrix due to signal and R_n is the noise autocorrelation matrix. Since we have assumed noise of variance σ^2 added to the signal, the entries of the noise autocorrelation matrix will ideally be equal to the variance of noise. We then decompose R_X into its corresponding eigen values (λ_i's) and eigen vectors $\left(V_i \text{'s} \right)$, with the eigen values arranged in decreasing order:

$$\lambda_1 \geq \lambda_2 \geq ..... \geq \lambda_P \geq \lambda_{P+1} = \lambda_{P+2} = ...\lambda_M = \sigma^2 \qquad (3.6)$$

where R_X is of dimension M x M and p represents the number of complex exponentials in the received data. It is easy to find p from the eigen values of R_X. Furthermore, the eigen vectors corresponding to the minimum eigen values are orthogonal to those of

the signal vectors. Taking a Fourier transform of the coefficients in V_i, we have [15]

$$v_i\left(e^{j\omega}\right) = \sum_{k=0}^{M-1} v_i(k)\, e^{-jk\omega} = e^H v_i \qquad (3.7)$$

(where $i = p+1, p+2,...., M$) will yield zeros at the frequencies of complex exponentials, or conversely, the function

$$P_{music}\left(e^{j\omega}\right) = \frac{1}{\sum_{i=p+1}^{M}\left|e^H v_i\right|^2} \qquad (3.8)$$

will yield sharp peaks at the frequencies of the corresponding frequencies. A weighted average of the all-noise eigen vectors is used so that spurious peaks arising out of individual noise eigen vectors may be suppressed [15].

3.2 Simulation test results

The profile of Table 3-1 was applied to MUSIC and the location of the p largest peaks are chosen as the unknown frequencies in the signal. Figure 3-2 shows a bar chart of the eigen values of R_X arranged in descending order. It can be seen that there are 4 significant eigen values and we chose p to be 4. Figure 3-2 shows the frequency spectrum obtained by using (3-8).
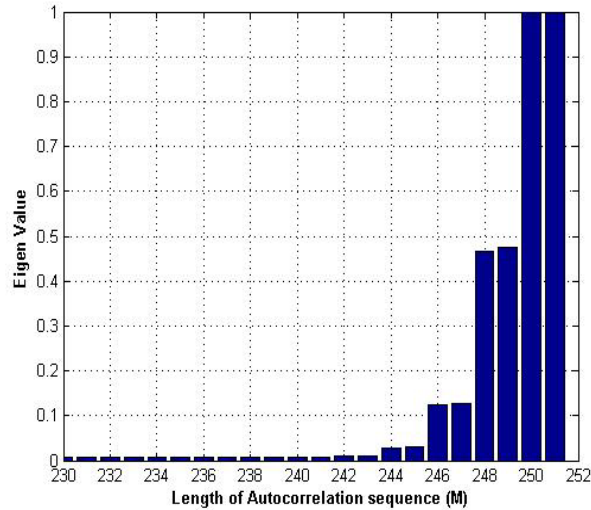
Figure 3-2 Selecting the number of complex exponentials *'p'*
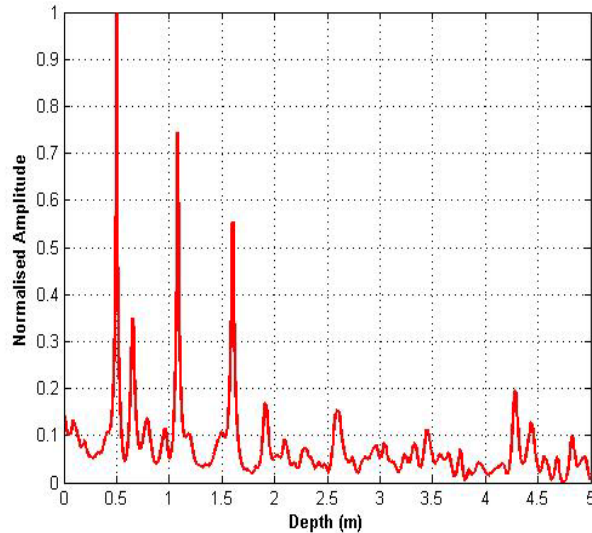
Figure 3-3 Range profile of table 3.1 plotted using MUSIC

Figure 3-3 shows that the resolution obtained using MUSIC is much better than that shown in Figure 3-1, which uses the FFT. We see that MUSIC is able to resolve all the four peaks very well and gives us an enhanced reflectivity profile.

To further demonstrate the resolution capability of MUSIC, we consider a 5-layer profile (with permittivities of 1, 3.4, 3.7, 2.9, 2.7 varying with depth) and the radar return signal is modeled such that the SNR is set to be 0 dB. Figure 3-4 shows the range profiles obtained using the FFT and MUSIC methods.
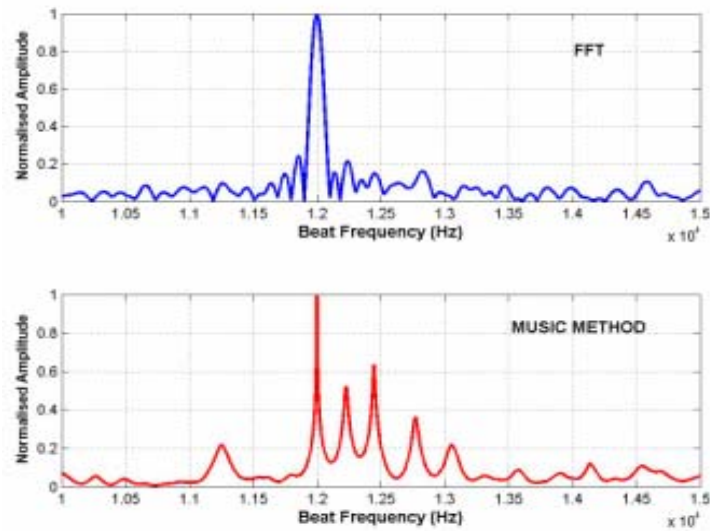
Figure 3-4 FFT Vs Spectral Estimation Algorithm for enhancement of Profile

It can be seen that FFT is unable to resolve the reflections due to very small permittivity contrasts (3.4 to 3.7 and 2.9 to 2.7). The side-lobes of the stronger reflections are clearly masking the weaker returns. The same figure shows the range profile obtained using MUSIC, where we find that this technique can effectively be used to enhance weak radar returns.

The performance of MUSIC is limited by the signal to noise ratio of the observed data. Simulations were performed on a large number of test cases and it was found that MUSIC performs well only for SNRs greater than 5 dB. Low SNRs result in incorrect estimates of p and hence, we do not have the "ideal" autocorrelation matrix of (3.5). If the estimated number of frequencies is less than the true value p, the frequency estimation function does not show all the frequencies in the signal, whereas for estimated values greater than p, spurious peaks appear in the spectrum. However, in a practical radar measurement, an SNR of 10-15 dB is reasonable and hence MUSIC can be used.

The resolution capability of MUSIC holds several applications such as studies relating to the sea-ice and snow where we wish to obtain enhanced reflectivity images to map the bedrock of ice and to detect faint internal layers of snow.

Now that the problem of profile enhancement has been addressed using MUSIC, we now proceed to the problem of data inversion or inverse permittivity profiling.

Chapter 4

Inverse Permittivity Profiling

Inverse permittivity profiling is a problem where the unknown parameter (permittivity) needs to be estimated from the received radar data. More specifically, for this work, we are interested in estimating unknown permittivity values given the data measured by a Ground Penetrating Radar. This problem is also called *Electro-Magnetic Inversion* or *EM parameter Estimation*.

Typically, inverse problems deal with estimating parameters based on continuous-time signals. However, modern radar systems use digital computers to sample and store analog waveforms, and hence we have the equivalent problem of extracting parameter values from a discrete time waveform or a discrete data set [16]. Mathematically, let us assume that the data set $Y = \{y[0], y[1], ..., y[N-1]\}$ represents the sampled version of the observed data, where N is the number of samples in the waveform. This data set depends on an unknown parameter *m* and we wish to determine the set of values *m* based on the data set *Y*. For the radar data inversion problem, the data set denoted by *Y* is the data obtained from a GPR; $\hat{m}$ translates into the set of permittivity values $\hat{\varepsilon}$ (permittivity values) that we wish to estimate. We will now discuss methods for data inversion.

4.1 Inversion by Layer Stripping

Layer stripping is an elementary approach for data inversion [17]. Let us assume that we have eliminated clutter from the observed data. Hence, ideally, we are left with a

delayed and attenuated version of the transmitted signal. As mentioned earlier, the Fast Fourier Transform (FFT) algorithm is applied on the received waveform to obtain the spectrum of the signal. A plot of this signal with respect to the distance axis will show the occurrence of peaks at interface locations. Ideally, the amplitudes of these peaks will correspond to the reflection coefficients (and transmission coefficients) at their respective interface locations. That is, the amplitude of reflected signal at any layer **k** is given by Equation 4.1 as

$$A_k = B_k \sum_{k=1}^{L} \Gamma_k \prod_{j=1}^{k} T_j \qquad (4.1)$$

where B_k represents the attenuation coefficient, which accounts for losses due to absorption, scattering and spreading. However, modeling the attenuation coefficient requires some *a priori* information regarding the properties of the target. Hence, for our inversion problem, we will assume that the lossy part of the medium (which contributes to the attenuation coefficient) is known. We also assume that the transmission coefficient for the first layer (air) $T_1 = 1.$ The "ideal" amplitude of the surface reflection will be $\Gamma_1 T_1$, the subsequent layers will have amplitudes $\Gamma_2 T_1 T_2$; $\Gamma_3 T_1 T_2 T_3$ and so on. The locations of their corresponding distances are directly related to their respective time delays. If Z_0 represents the height of the surface from the antenna and Z_k represents the depth of the kth layer in a multi-layered media of **L** layers, the two-way time delay τ_k experienced by the signal is given as

$$\tau_k = \frac{2}{c}\left[z_o + \sum_{i=1}^{k} (z_i - z_{i-1})\sqrt{\varepsilon_i} \right] \qquad (4.2)$$

The idea in layer stripping is that we first identify the amplitudes (A_k's) and the locations of interfaces (τ_k's) from the range profile of the received signal. Once these values are known, it is easy to determine unknown variables (permittivity values) recursively using Equations (4.1) and (4.2).

The first task is the detection of echoes. This is done by setting a reasonable threshold amplitude value based on the Signal-to-Noise ratio (SNR) of the system. All amplitudes that cross this threshold are picked as valid returns. The positions corresponding to these returns constitute the distances (delays). These values are used to recursively estimate the permittivities.

However, since the detection of echoes is performed without any reference to a geophysical model, this approach suffers from the following limitations.

1. **Missed Peaks:** Since the detection of echoes is done by setting a threshold by looking at the range profile, the value of the threshold is important. In certain profiles consisting of small dielectric variations, the reflection at that interface could be very small and could be embedded in noise. Hence, without any knowledge of the profile, an arbitrary threshold value might cause missing of that peak. Therefore, this leads to an error in the estimated permittivity profile.

2. **False Alarms:** In many cases, we might not be able to distinguish between actual signal peaks and false alarms – which are unwanted reflections that arise due to the presence of random noise or reflections due to clutter/external factors. The selection of false alarms as signal peaks can also lead to erroneous permittivity profiles.

3. **Range Sidelobes:** To obtain the range profile, the Fourier transform algorithm is usually applied on the IF beat signal measured by an FMCW radar. But this method

suffers from the problem of range sidelobes. That is, the weaker reflections (smaller reflection coefficients) are masked by the sidelobes of stronger reflections. Hence, this presents a serious impediment when identifying valid peaks from the range profile for data inversion.

To illustrate the performance of the layer stripping approach, simulations on an FMCW radar are presented here. Consider a geoprofile along with radar parameters as tabulated in Table 4-1.

Table 4-1 Radar and geophysical parameters to illustrate layer stripping

Bandwidth	6 GHz
Start Frequency	2 GHz
Sweep time	10 ms
Chirp rate	300 GHz/s
SNR	10 dB
Permittivity vector ε_r	[1 1.5 1.9 1.5]
Depth vector $\mathbf{Z}$ (cm)	[8 4 8]

The range profile for this multilayered structure was modeled using MATLAB and is shown in Figure 4-1 below.
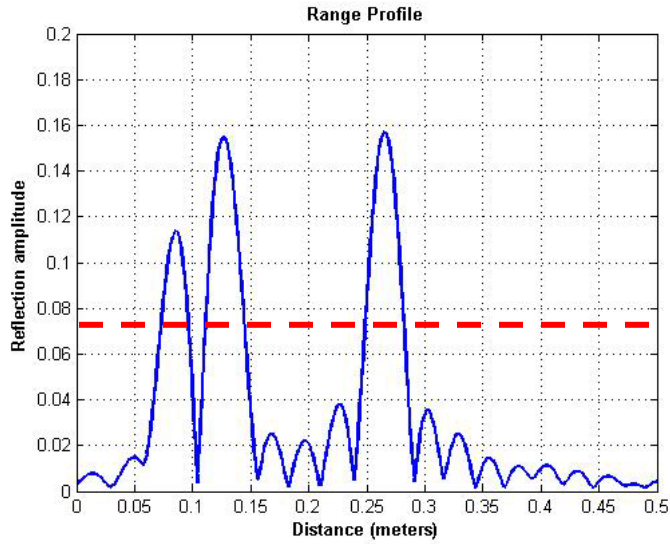
Figure 4-1 Range Profile obtained using FFT

From the permittivity vector of Table 4-1, there are four dielectric interfaces and hence we see three peaks in the Figure 4-1. As discussed in Chapter 2, the amplitudes of these peaks correspond to the reflection coefficient of the interface. To estimate the permittivities, we need to set a reasonable threshold. In this case, intuitively, it can be seen that a safe value of 0.07 can be chosen based on the relative amplitudes of signal and noise. (This is indicated by the dashed line in the same figure). Here, it is interesting to note that the interface locations are slightly different from the actual locations. This is because the velocity of the EM wave in every layer is different and it depends on the permittivity of that particular layer. The interface locations are estimated from the change in slope from negative to positive. From the reflection coefficient values, the permittivities can be calculated by recursively using the formulae discussed in Chapter 3. The final reconstructed profile is shown in Figure 4-2 below.
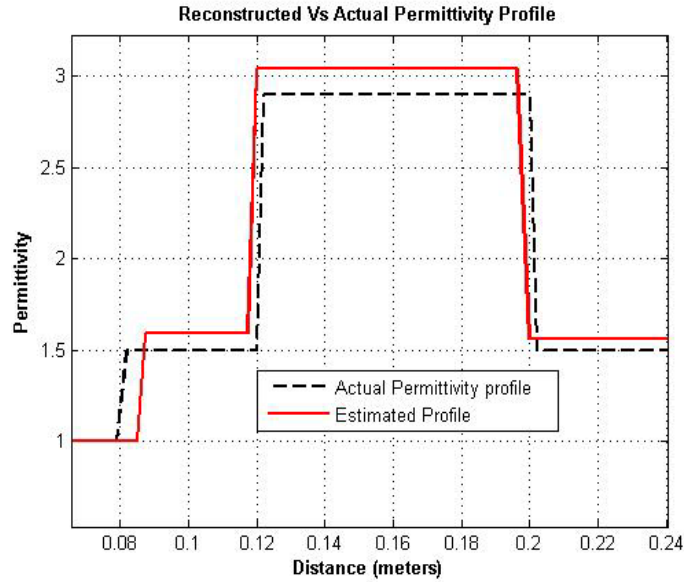
Figure 4-2 Actual Vs Reconstructed Permittivity Profile

The importance of setting a reasonable threshold is obvious. To illustrate this, we now consider a profile shown in Table 4-2 below to explain the problem of false alarms and missed peaks.

Table 4-2 Profile chosen to illustrate the problem of false alarms and missed peaks

Permittivity vector ε_r	[1 3 3.5 2 2.8]
Depth vector $\mathbf{Z}$ (cm)	[50 30 40 40]
SNR	5 dB

Figure 4-3 depicts the range profile modeled as in the previous example. As we can see, this data is noisy. The peaks which are checked are valid peaks. To illustrate the problem of missed peaks and false alarms, three thresholds marked as 1, 2 and 3 are set as shown in the figure.

31
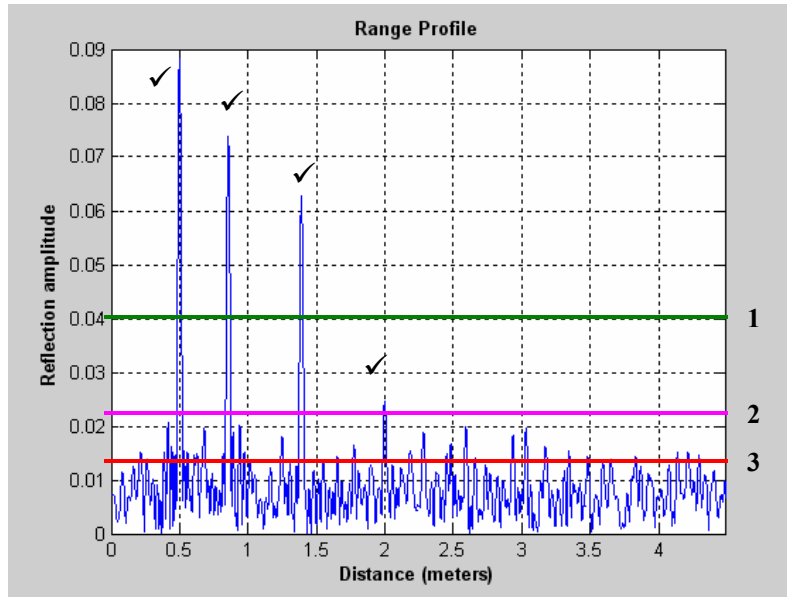
Figure 4-3 Range Profile of Table 4.3 with thresholds marked

If a threshold corresponding to 1 is set, only the first three peaks will be above the threshold and hence we miss the last peak corresponding to the return from the last interface. This is the problem of *missed peaks* in threshold detection. Hence, the reconstructed profile will not show the last layer.

However, if the threshold is set a value given by 2, all four valid peaks will be detected and we can invert the profile very well. But, if the threshold is set at the value indicated by 3, then several peaks will be detected, apart from the valid peaks. These unwanted peaks are called *false alarms* and these will result in incorrect permittivity profiles.

4.2.1 The Problem of sidelobes:

In Chapter 3, we discussed the problem of the FFT's inability to resolve closely spaced reflections because of the masking of weak reflections by the sidelobes of the stronger reflections. Thus, the problem discussed above imposes a limitation on the

robustness of the method. The following example illustrates this point. Let us consider a profile as tabulated in Table 4-3 below and the range profile shown in Figure 4-4.

Table 4-3 Profile chosen to illustrate the problem of sidelobes

Permittivity vector ε_r	[1 3.4 3.7 2.9 3.7]
Depth vector **Z** (cm)	[50 8 20 30]
SNR	15 dB
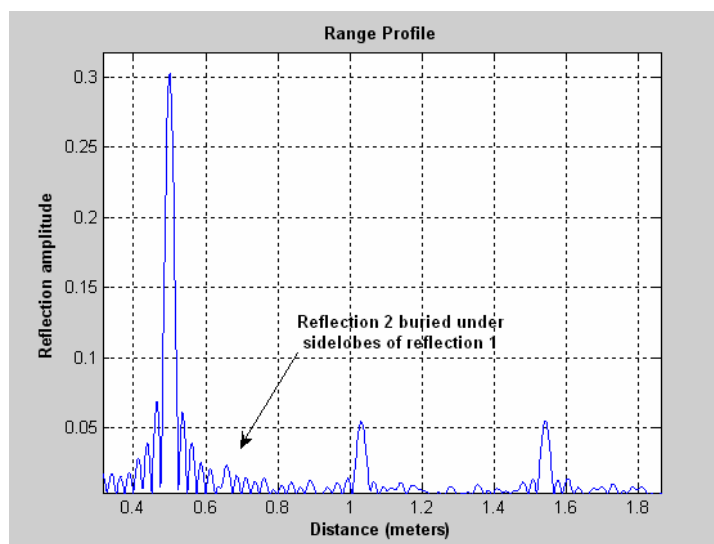
Figure 4-4 Range profile of table 4-4

Here, we find that, though the SNR of the signal is good, the reflection off the second interface is weak and is masked by the sidelobes of the reflection from the first layer. Hence, layer stripping fails to detect this buried reflection, and as a result the estimated permittivity profile will look distorted.

Hence, we see that the layer stripping method is useful only when the SNR of the signal is good enough and when the peaks can be sufficiently resolved. Also, it requires the setting of a reasonable threshold value to distinguish between false alarms and valid

peaks. This method is also vulnerable to errors because of the problem of sidelobes masking the weak returns. Hence, we find the need for a more robust parameter estimation algorithm – preferably one which incorporates the underlying physical phenomenon. Nevertheless, the layer stripping technique can be used as a first step to get an approximate inverse solution.

4.2 Model Based Inversion

Stergiopoulos [18] suggests that, if the physical phenomenon is incorporated into the algorithm, the inversion results are better. Such an estimator, which uses the geophysical model to estimate unknown parameters, is called a *model-based estimator.* The concept of model-based estimation was depicted earlier in Figure 1-2.

This geophysical model is the forward model which was discussed in Chapter 2. It was seen that there exists a non-linear relationship between the observed data and the unknown permittivity values. From a mathematical point of view, these types of problems may be solved by using non-linear regression techniques based on certain criteria. A widely used criterion is the minimization of mean squared error for estimation of unknown parameters [19].

4.2.1 MMSE Minimization techniques

In this method, we attempt to minimize the squared difference between the observed data Y (given by Equation 3.2) and the assumed signal model or noiseless data F, which is a function of the unknown parameter m. This concept is illustrated in Figure 4-5 [19].

A fundamental assumption in this approach is that the signal $F(m,n)$ is purely deterministic. As discussed earlier, due to random noise or model inaccuracies, we observe a perturbed version of $F(m,n)$, which is denoted as Y. The MMSE estimator of m chooses the value that makes $F(m,n)$ closest to the observed data $Y(n)$.

(a) Data Model

(b) Least Squared error
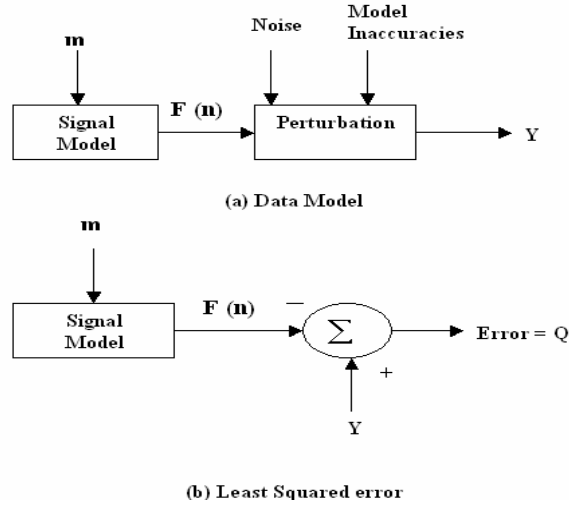
Figure 4-5 The Least Squares Approach

Closeness is quantified by the least squared error criterion given by Equations (4.3) and (4.4) below

$$Q = \sum_{n=0}^{N-1}(Y(n)-F(m,n))^2 \qquad (4.3)$$

OR

$$Q = \|Y(n)-F(m,n)\|^2 \qquad (4.4)$$

where the observation interval is assumed to be **n = 0, 1 ,…, N-1.** The value of m that minimizes Q is the MMSE estimator of m. The performance of this method depends upon the properties of the corrupting noise as well as other external and internal sources

of error in the system and in the observation. We will now explore the Gauss Newton Method, which is based on MMSE minimization.

4.2.1.1 Gauss Newton Method

As mentioned earlier, there is a non-linear relationship between the signal model and the model parameters. Non-linear least squares problems cannot be solved directly; they must first be converted into linear form. The iterative Gauss Newton method [17] gives a solution by linearizing the model $F(m, n)$ about some nominal m and then uses the linear least squares procedure as described in [15,16].

$$F(m) \cong F(m_c) + \left[\nabla_m F(m_c) \right](m - m_c) \qquad (4.5)$$

where $\nabla_m F(m_c)$ indicates the matrix of partial derivatives of $F(m)$ with respect to model parameters evaluated at $m = m_c$. The variable m_c denotes the set of current model parameters. Revisiting Equation (4.3), we can derive the solution of the non-linear problem as follows.

$$Q = \sum_{n=0}^{N-1} \left(Y(n) - F(m, n) \right)^2 \qquad (4.6)$$

$$\approx \sum_{n=0}^{N-1} \left(Y(n) - F(m, n) + \frac{\partial F[m, n]}{\partial m} \bigg|_{m=m_0} m_0 - \frac{\partial F[m, n]}{\partial m} \bigg|_{m=m_0} m \right)^2 \qquad (4.7)$$

To initiate the algorithm, we begin with a starting guess for the model parameters, denoted by m_0. Proceeding further, Equation (4.7) can be written as

$$Q=\left[Y-F(m_0)+H(m_0)m_0-H(m_0)m\right]^T * \left[Y-F(m_0)+H(m_0)m_0-H(m_0)m\right]$$

$$(4.8)$$

where we define **H** as the matrix of partial derivatives of the modeled data with respect to the model parameters **m**. Now since we have a linear model, we can use the theory of least squares error minimization where the model updating is obtained by back projecting the residual i.e., $Y-F(m)$ onto the model space to obtain the solution. Equation (4.8) can be solved to obtain the least square error estimate as:

$$\hat{m}=\left[H^T(m_0)H(m_0)\right]^{-1}H^T(m_0)\left[Y-F(m_0)+H(m_0)m_0\right] \quad (4.9)$$

$$= m_0 +\left[H^T(m_0)H(m_0)\right]^{-1}H^T(m_0)\left[Y-F(m_0)\right] \quad (4.10)$$

This can be iterated so that

$$m_{k+1}=m_k + \left[H^T(m_k)H(m_k)\right]^{-1}H^T(m_k)\left[Y-F(m_k)\right] \quad (4.11)$$

4.2.1.2 Limitations of the Gauss-Newton Technique

Methods of parameter estimation such as the Gauss-Newton MMSE algorithm and Minimum Variance Unbiased (MVU) estimate algorithm, which are iterative procedures, suffer from convergence problems. As discussed earlier, the algorithm produces an estimate $\hat{m}$ that minimizes the mean squared difference Q between the observed and the model parameters. To find the optimum estimate, the algorithm is initiated with a starting guess m_0 or, for convenience, $m^{(1)}$ and then we sequentially find $m^{(2)}, m^{(3)},...$ in such a way that the sequence finally converges to $\hat{m}$ - which

yields the minimum mean squared error. This process is called convergence and the value of MMSE obtained is called the *global minimum*.

In simple mathematical terms, a global minimum of a function is the lowest value that the function achieves. In our case, this function is the error function that we are trying to minimize. If we assume the function to be a surface, then a global minimum is the lowest point on that surface. MMSE minimization algorithms are typically based upon a quadratic approximation to the error function $Q(m)$. Seber [16] suggests that the Newton method will converge provided the starting guess $m^{(1)}$ is close enough to the estimate $\hat{m}$. However, in a few cases, global minimum convergence is not achieved. The algorithm could result in a local minimum.

Apart from the problem of local minimum convergence, MMSE methods at times, do not converge at all. Again, as in the local minimum case, convergence is sensitive to the starting guess. A bad starting value can either result in a local minimum or may never converge at all. However, MMSE minimization techniques are still widely used to solve non-linear problems because they can fit a broad range of functions. Also, they produce good estimates of the unknown parameters in the model with relatively small data sets [19].

A simple but time-consuming approach to circumvent the problem of convergence is to run this algorithm with several starting guess values and select the case with the least error. Also, the model parameter values at every iteration need to be constrained and should not be permitted unlimited freedom of movement. A few methods of constrained optimization for non-linear regression are available in [16,20]. However, convergence cannot be guaranteed.

Convergence was also found to be highly dependent on the SNR. Simulations on various test cases showed that the convergence results are very poor for SNRs less than 15 dB. Hence, the Gauss Newton method was not found to be a reliable technique for our problem. There are other regression based techniques which are iterative and they too suffer from the aforementioned problems.

Hence, it was decided to follow a two-step model-based approach: first, the estimation of unknown frequencies in the signal, and second, the estimation of amplitudes of the corresponding frequencies.

4.2.2 Inversion based on Spectral Estimation

The first step can be achieved by using the MUSIC algorithm and the second by using a suitable estimator, such as a maximum likelihood estimator [21]. Referring to (3.1), we first estimate ω_k's using (3.8). We are now left with the problem of estimating A_k's. Formulating the received signal of (3.1) in a vector form as

$$
\begin{bmatrix} x(0) \\ x(1) \\ : \\ : \\ x(N-1]) \end{bmatrix} = \begin{bmatrix} 1 & \cdots & 1 \\ e^{j.f(\omega_1)} & \cdots & e^{j.f(\omega_k)} \\ : & : & \cdots \\ : & & \\ e^{j(N-1).f(\omega_1)} & \cdots & e^{j(N-1).f(\omega_k)} \end{bmatrix} \begin{bmatrix} A_1 \\ A_2 \\ : \\ : \\ A_k \end{bmatrix} + \begin{bmatrix} w(0) \\ w(1) \\ : \\ : \\ w(N-1) \end{bmatrix} \quad (4.12)
$$

where W represents additive white Gaussian noise, the unknown amplitudes A_k's may be estimated as [22]

$$
\hat{A} = \left(\hat{S}^H \hat{S} \right)^{-1} \hat{S}^H . X \quad (4.13)
$$

where $\hat{S} = \sum_{k=1}^{P} e^{j \cdot f(\omega_k)}$, obtained from the estimated frequencies using MUSIC. Under

the assumption of white Gaussian noise, $\hat{A}$ turns out to be the maximum likelihood

estimator of A [21]. However, it is difficult to confirm the properties of noise. Yet, it may

be called an unbiased estimator for $\hat{A} = A$ [22]. There are other methods to estimate

unknown amplitudes from signals corrupted by non-Gaussian noise. Chen [23] suggests a

projection matrix decomposition approach to estimate sinusoidal parameters from colored

noise. We may also use a pre-whitening filter to convert colored noise to Gaussian noise;

hence we may use (4.13) for amplitude estimation. Using Equations (4.1) and (4.2)

recursively, we can estimate the permittivities of each of the layers.

We now present a few simulations using the MUSIC algorithm. The input

parameters for this algorithm are the radar parameters (such as start frequency,

bandwidth, chirp rate, time of sweep, number of samples), number of snapshots of data,

the number of subarrays and number of time delay components (or equivalently the

number of sinusoids present in the signal).

Let us consider the profile of Table 4.2, but with an SNR of 10 dB. As discussed

earlier, the first step is the enhancement of the range profile. Figure 4-6 compares the

FFT range profile with that obtained using MUSIC.
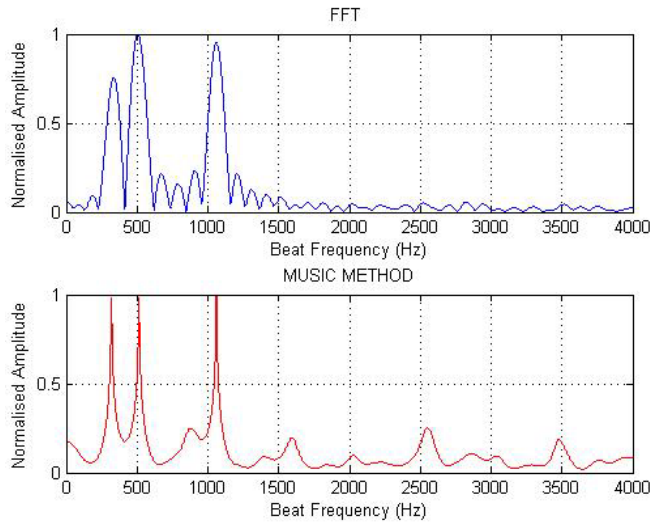
Figure 4-6 Range profiles obtained using FFT and MUSIC for profile of Table 4-2

It is clearly seen that the resolution is much better using MUSIC where the three signal peaks are well defined. From this profile, the corresponding beat frequencies were identified and fed into the amplitude estimation module.
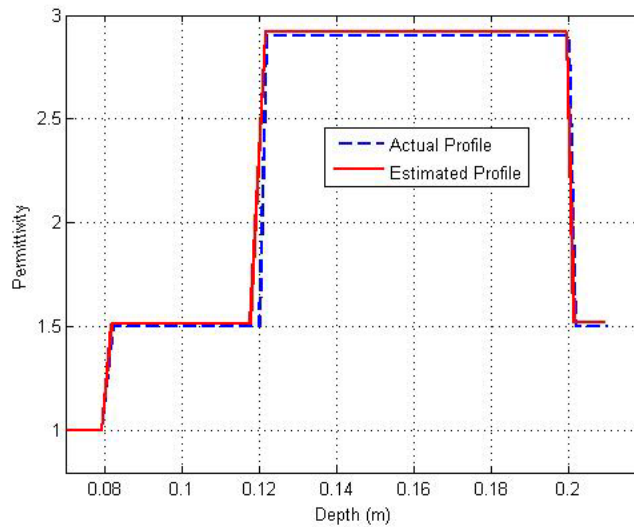
Figure 4-7 Reconstructed Vs assumed profile of Table 4-2 using MUSIC algorithm

The estimated set of parameters match really well with the true parameters and the reconstructed profile is plotted in Figure 4-7.

Let us now move on to consider a case where the distances are taken at random and are not constrained (Table 4-4) . Also, the SNR in this case is 5 dB.

Table 4-4 Geo-profile to test MUSIC with random depth profiles

Permittivity vector ε_r	[1 1.5 2.9 1.5]
Depth vector **Z** (cm)	[7.3 13.4 87]
SNR	5 dB

Figure 4-8 compares the range profiles using FFT and MUSIC. After identifying the beat frequencies corresponding to valid peaks, the permittivity profile is reconstructed and is shown in Figure 4-9.
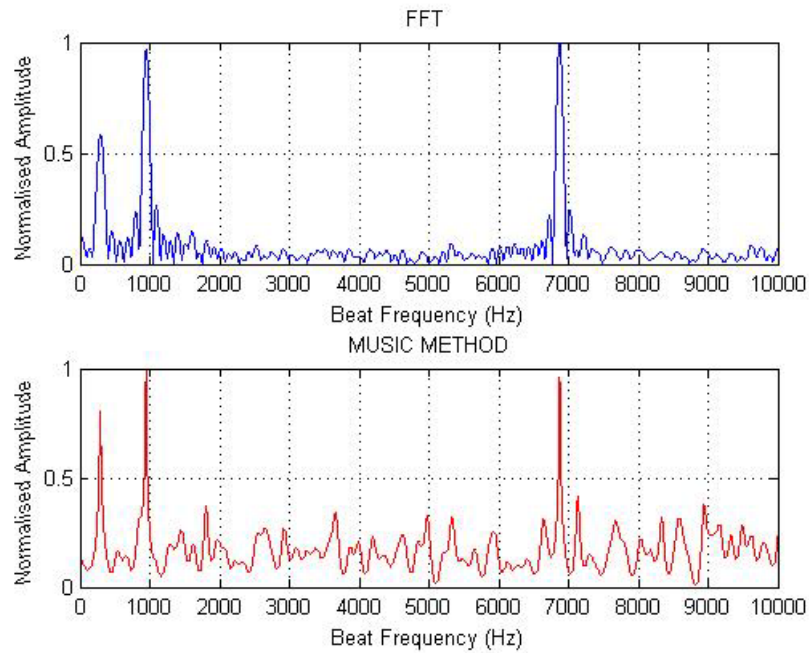
Figure 4-8 Range Profiles obtained using FFT and MUSIC for profile of Table 4-9
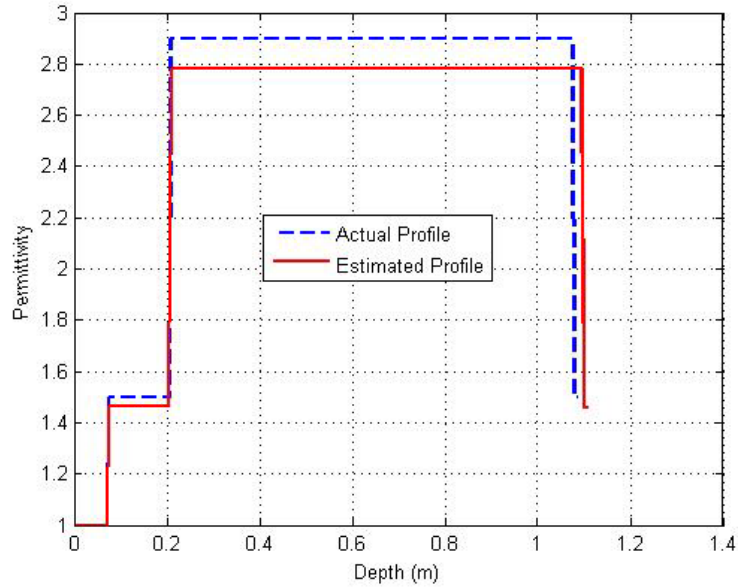
Figure 4-9 Reconstructed Vs actual permittivity profile of Table 4-9

Hence, we find that MUSIC works well irrespective of the distribution of the depth profile. Next, let us consider a more complicated scenario (Table 4-5) characterized by very subtle variations in permittivity and a random depth distribution, which we can expect in a typical GPR field measurement.

Table 4-5 Geo-profile to test MUSIC with the problem of sidelobes

Permittivity vector ε_r	[1 1.5 1.7 1.9 5 3.5 7
Depth vector **Z** (cm)	[13 5 7.5 4 5 4.7]
SNR	10 dB

The range profiles using FFT and MUSIC are compared in Figure 4-10 below.
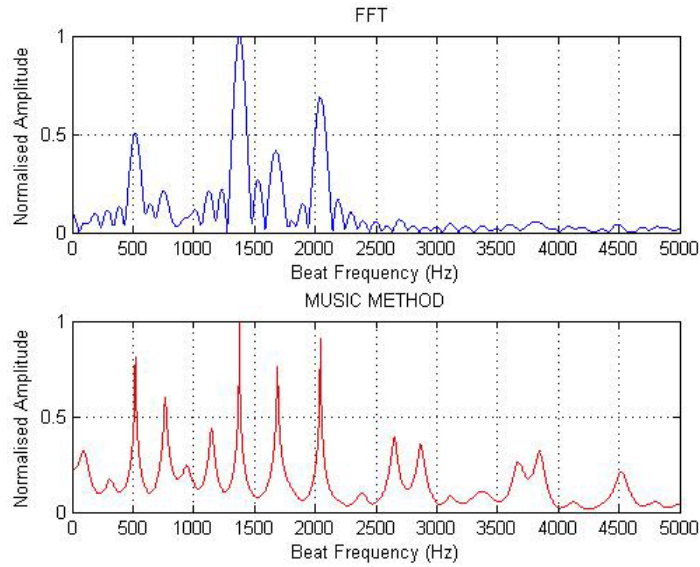
Figure 4-10 Range Profiles using FFT and MUSIC of Table 4-5

In the FFT profile, we find only four distinctly identifiable peaks due to the sidelobe-masking phenomenon discussed in Chapter 3. However, using MUSIC, we are able to resolve all the valid signal peaks. Figure 4-11 below shows the reconstructed permittivity profile after feeding the beat frequency values into the estimator.
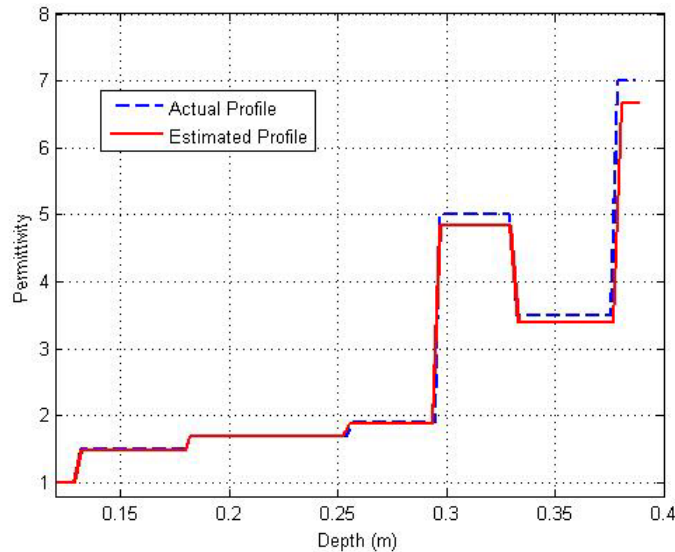
Figure 4-11 Reconstructed Vs assumed profile of Table 4-5

So far the algorithm has been successful in estimating permittivities in cases of poor SNR and for any distribution of profile – when the right beat frequencies are chosen. To test the robustness of this algorithm, let us now explore what the implications are when:

1. Noise peaks are chosen; and

2. Signal peaks are missed

The following test demonstrates this idea. Let us consider the MUSIC-enhanced profile of the earlier example shown in Figure 4-12 below.
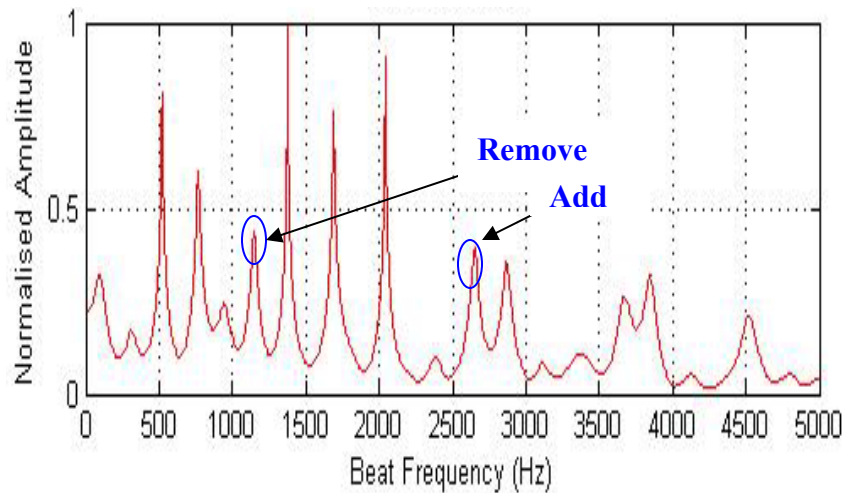
Figure 4-12 Range profile (using MUSIC) depicting enhancement of weaker reflections

We shall now make two changes to the beat frequency values fed into the estimator. First, the beat frequency corresponding to 1147.5 Hz will be removed (missed peak) and the beat frequency corresponding to 2654 Hz will be added (false alarm case). Now, with the new set of beat frequency values, we tested the algorithm, and the reconstructed profile obtained is shown in the Figure 4-13.
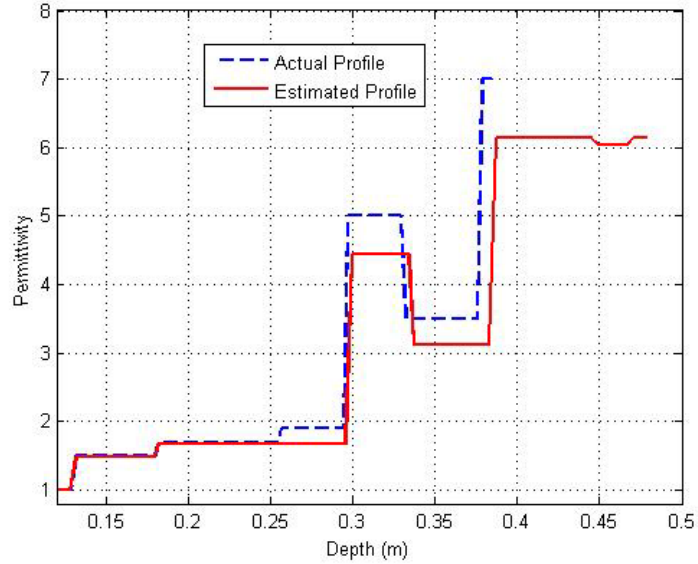
Figure 4-13 Reconstructed profile obtained after including false alarms in the beat frequency vector

The reconstructed profile shows that the profile looks slightly distorted. The selection of false alarms and missed peaks does not drastically alter the reconstructed profile.

In summary, the performances of the layer stripping approach, Gauss Newton method and the MUSIC algorithm were analyzed for permittivity profile reconstruction. Various cases were considered to test the algorithm for robustness, and it was seen that layer stripping works well only under certain conditions; the Gauss Newton method is not suitable due to convergence issues; and the MUSIC algorithm performs well for various test cases (radar data with low SNRs, radar profiles with very subtle changes in permittivity and profiles with random distribution of depth). In the next chapter, we will apply the MUSIC algorithm to invert actual radar data obtained from field experiments.

Chapter 5

Experimental Results

In chapter 4, a few methods for inversion were analyzed through simulations and it was seen that the performance of the MUSIC methods is better than the other methods. In this chapter, we will perform inversion on actual radar data collected from:

1. Field experiments conducted by the Radar Systems and Remote Sensing Laboratory (RSL) in Antarctica during the 2003 field season

2. Sandbox experiments at the RSL lab.

3. Field experiments conducted by the RSL in Greenland during the 2004 field season.

5.1 Experiments in Antarctica

The RSL at the University of Kansas used an Ultra Wide-Band (UWB) Frequency Modulated Continuous Wave (FMCW) radar to determine snow thickness over sea ice. We will use data collected during the 2003 field season in Antarctica to validate the working of the inversion algorithm. The estimated permittivity profiles will be compared with profiles obtained from *in situ* snow-pit measurements. A model of the snow radar system and the dielectric structure of the test site as given in [24] is depicted in Figure 5-1. The parameters of the UWB radar are tabulated in Table 5-1.
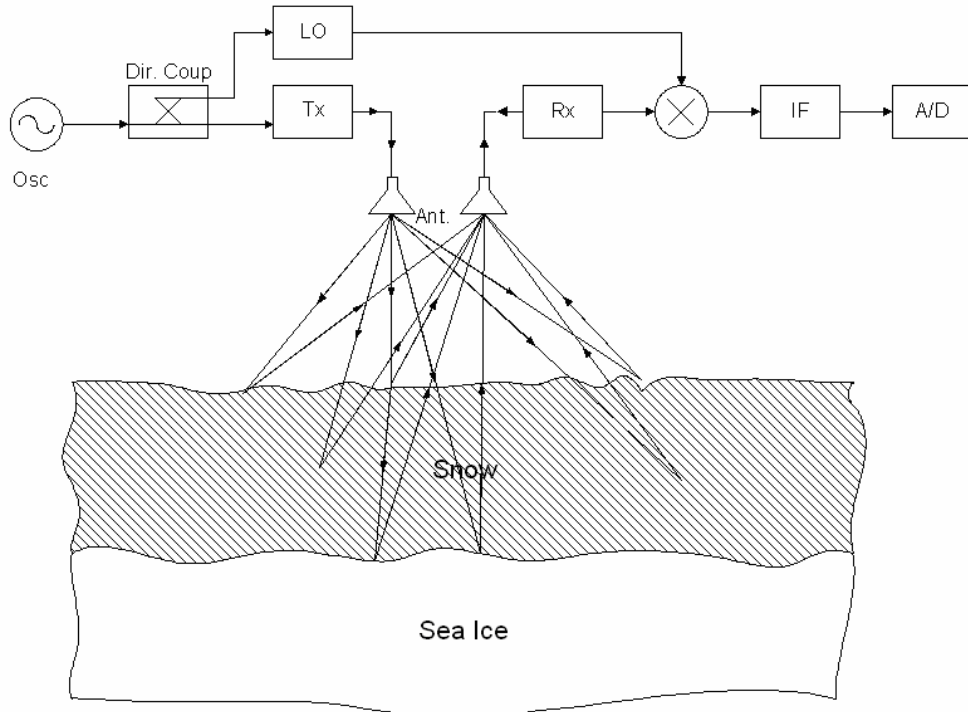
Figure 5-1 Model of the snow radar used in Antarctica.

Table 5-1 Parameters of UWB FMCW radar used in Antarctica

Characteristic	Value	Unit
Radar Type	FMCW	
Sweep Frequency	2-8	GHz
Range Resolution	$\cong 4$	cm
Sweep Time	10	msec
Transmit Power	13	dBm
PRF	25	Hz
Sampling Rate	5	MHz
Antenna	TEM Horn Antenna	

It can be seen that the dielectric structure consists of a layer of air, several layers of snow and a homogeneous layer of sea ice extending all the way down to the bedrock. Air is modeled with a permittivity of one. Sea ice can be modeled using the Tinga mixing model given in [9]. However, for simplicity, the permittivity of sea ice can be taken to be approximately 3.14 in the microwave frequency region. Modeling the permittivity of snow requires parameters such as density, wetness and other factors which can be obtained from snow-pit measurements. From these parameters, the complex permittivities can be calculated using appropriate mixing models from the literature [9]. Table 5-2 shows the *in situ* measurements taken at one of the test sites in Antarctica where the FMCW radar was tested. The models used to calculate the permittivites are discussed in Appendix A.

Table 5-2 Modeled core (in-situ) parameters

Layer Thickness (m)	Density (g/cm³)	Salinity [⁰/₀₀]	Wetness [Vol %]	$\varepsilon_{effective}$ (Modeled - Absolute) (from Appendix A)
1.83	1.40	0	0	1.00
0.03	0.191	0.145	-0.46	1.44
0.03	0.254	-	0.73	1.60
0.03	0.328	0.07	0.09	1.70
0.03	0.364	0.31	0.00	1.77
0.03	0.355	0.11	0.00	1.74
0.03	0.334	0.21	0.00	1.71
0.03	0.285	0.20	0.39	1.65
0.03	0.293	0.12	0.49	1.66
0.03	0.244	0.31	1.41	1.67
0.03	0.254	0.34	1.67	1.71
0.03	0.245	0.30	1.76	1.71
0.03	0.226	0.27	1.96	1.69
0.03	0.309	0.05	0.31	1.68
0.03	-	2.17	3.00	2.20
0.015	-	29.4	3.28	6.35

The permittivity profile of Table 5-2, modeled by using the empirical formulae in Appendix A, is plotted in Figure 5.2 below.

Having looked at the actual permittivity profile at the measurement site, we now apply the inversion algorithm on actual radar data measured at the same site. Figure 5-2 below shows the range profile of A-scope 20 plotted using FFT.
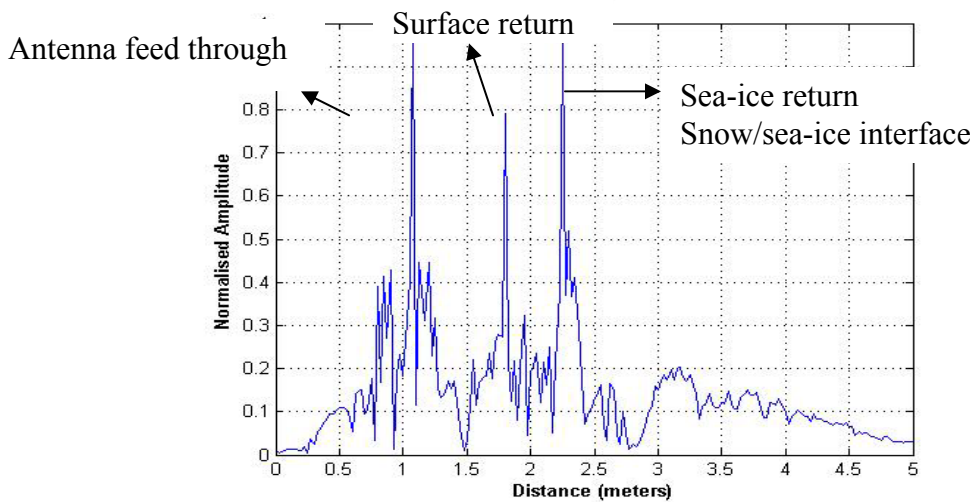
Figure 5-2 Range Profile plot of A-scope 20

From Figure 5-2, we can see three well defined peaks corresponding to

1. Antenna feed through return

2. Return from surface layer (Air/Snow interface) and

3. Return from snow/sea-ice interface

Apart from these peaks, there are other smaller peaks which correspond to internal snow layers. Before applying the inversion algorithm, the first step is to remove the radar system effects and the antenna feed-through using calibration data. A flat metal screen is used as the target, the return signal is collected, and the main peak (corresponding to the plate) is filtered out. The filtered signal now represents the impulse response of the system and is commonly used to account for system effects (which also include the

antenna response). The Fourier transform of this signal gives the transfer function of the radar system X(f) and can be eliminated from the observed return Y(f) using Equation 5.7 to yield the response of the target $\Gamma(f)$.

$$\Gamma(f) = \frac{Y(f)}{X(f)} \qquad (5.7)$$

The next step is to remove the antenna feed through by using a band-pass filter. The range profile after calibration and filtering is shown in Figure 5-3.
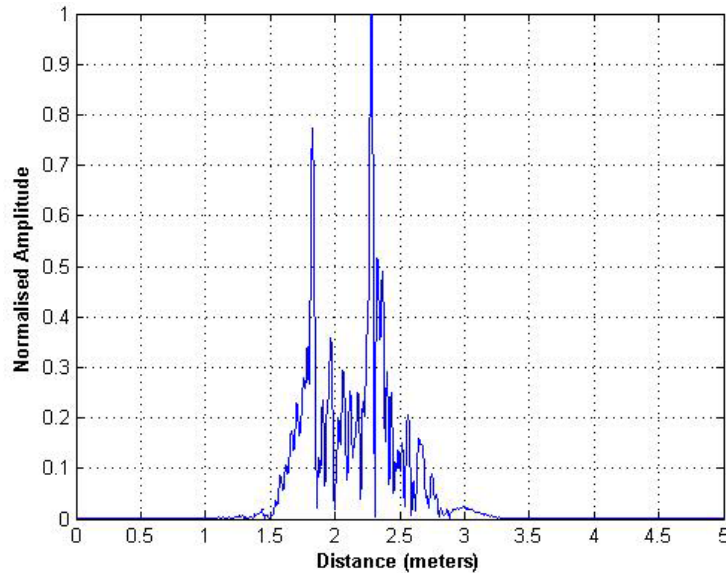
Figure 5-3 Range Profile after calibration and filtering

Now, the data can be fed into the inversion algorithm. Clearly, the reflections from internal snow layers need to be resolved. As seen in Chapter 4, we first apply MUSIC on this data and enhance the spectrum. Figure 5-4 compares the range profiles obtained using FFT and MUSIC.
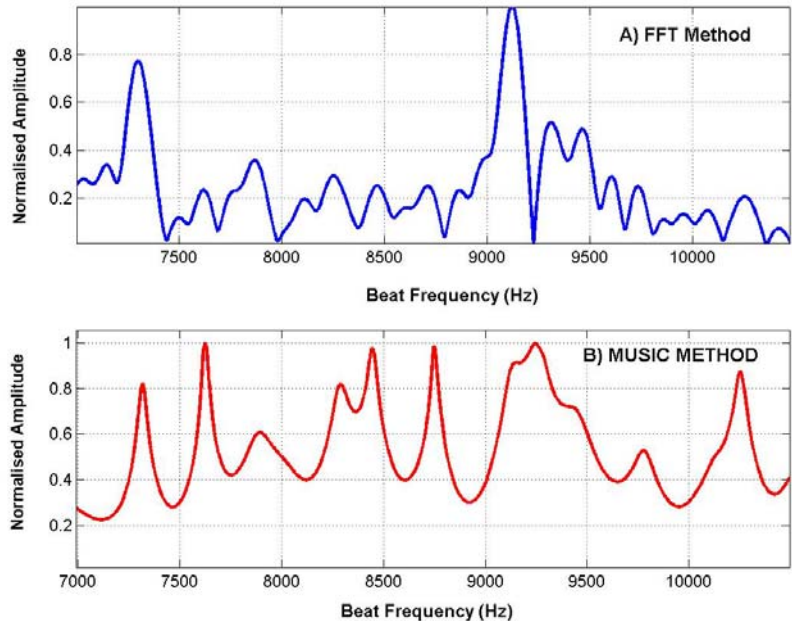
Figure 5-4 Range Profiles obtained using FFT and MUSIC

The beat frequencies detected from the enhanced range profile have been tabulated in Table 5-3 below.

Table 5-3 Comparison of estimated beat frequencies of core with those of FFT and MUSIC

Beat Freq F_B (Core data) Hz	Beat Freq F_B (*MUSIC*) Hz	Beat Freq F_B (IFFT) Hz
7320	7317.0	7290
7474	7622.0	7860
7630	7885.0	9120
7781	8290.0	
7936	8445.0	
8088	8748.5	
8243	9150.0	
8399	9240.0	
8559	9770.0	
8721		
8884		
9047		
9203		
9390		

These beat frequency values were fed into the estimator and the reflection coefficients were estimated. These values were then used to estimate the corresponding

52

layer permittivities by using Equations 2.1 and 2.2 recursively. The estimated permittivity

profile is plotted against the actual profile (modeled) in Figure 5-5 below.
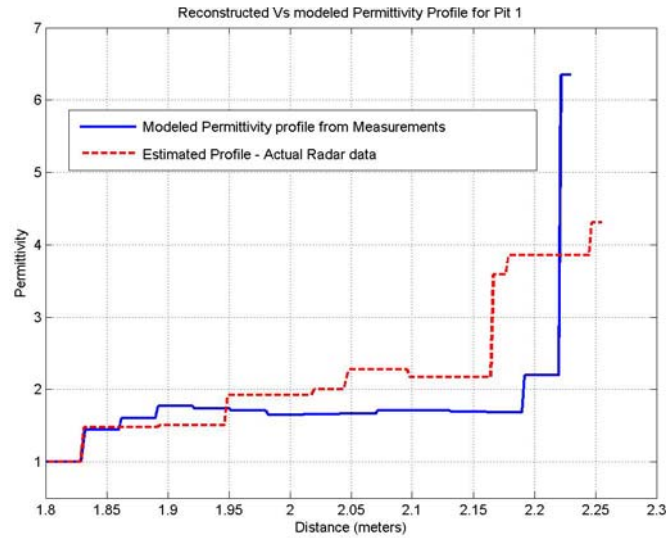
Figure 5-5 Reconstructed Vs modeled profile for Pit 1

As we can see from the above profile, the MUSIC-estimated profile matches

reasonably well up to a certain depth, but gradually deviates from the measured values, as

we move into deeper layers. This deviation is expected, because, at greater depths, the

signal is greatly attenuated because of significant salinity, as shown in column 3 of Table

5-2, which was not factored into the reconstruction of the permittivity profile.

Other variations in the estimated profile could be attributed to: (1) a discrepancy

in the model representing the radar return, (2) an error in calibration data, (3) very subtle

changes in the permittivity that MUSIC is not able to distinguish, and (4) measurement

errors in the field that cannot be compensated for at this stage, since we are using existing

data.

The algorithm was also tested at two other locations where measurements were

made using the same FMCW radar. Figure 5-6 shows the range profiles using FFT and

MUSIC on data measured at one of the pits (Pit 2) on September 28, 2003.
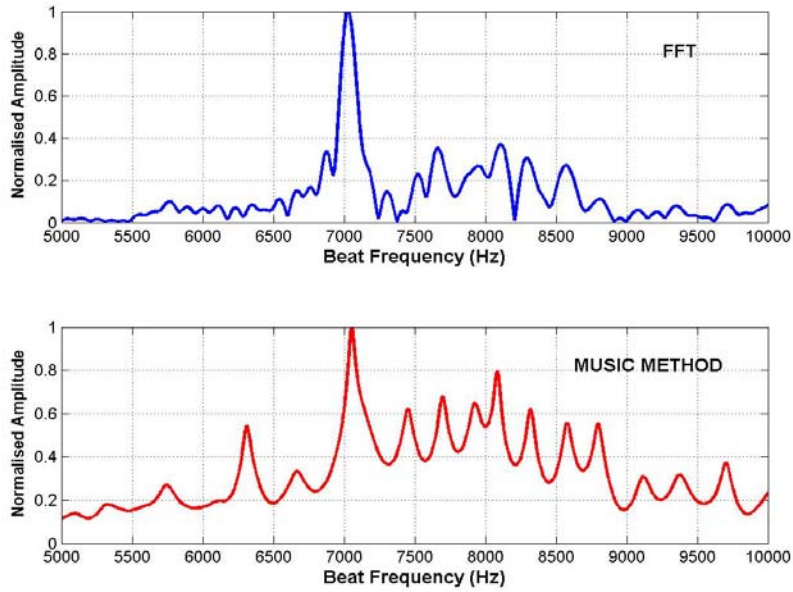
Figure 5-6 Range Profiles obtained using FFT and MUSIC for Pit 2

Following the same procedure, the reflection coefficients were estimated and the reconstructed permittivity profile is plotted in Figure 5-7.
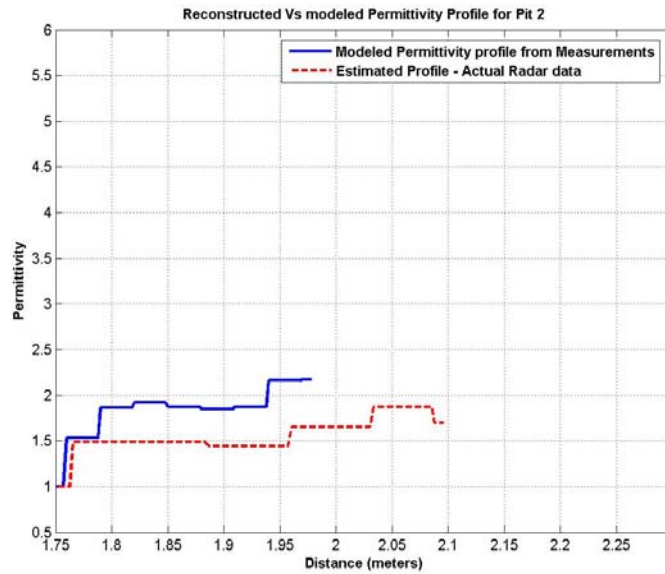
Figure 5-7 Reconstructed Vs modeled profile for Pit 2

Similarly, the algorithm was also tested on another location on October 14 (Pit 3). The range profiles and the reconstructed permittivity profiles are depicted in Figures 5-8 and 5-9 respectively.
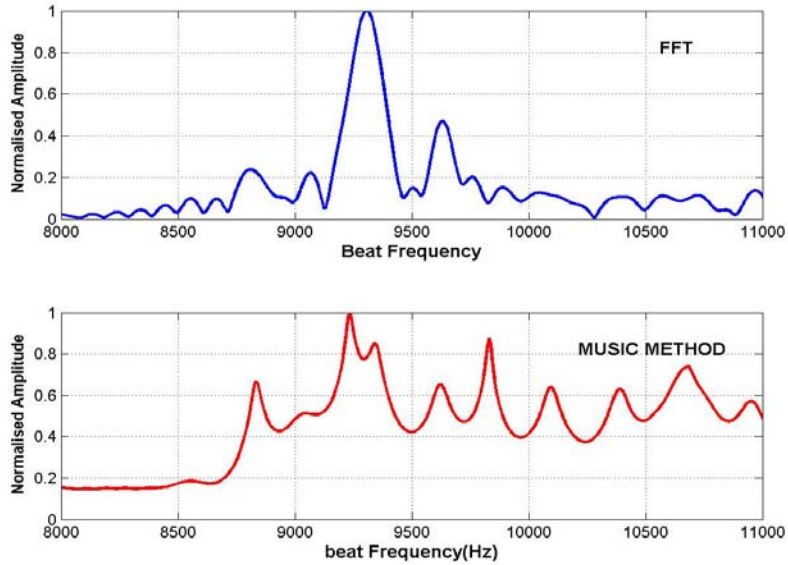
Figure 5-8 Range Profiles obtained using FFT and MUSIC for Pit 3
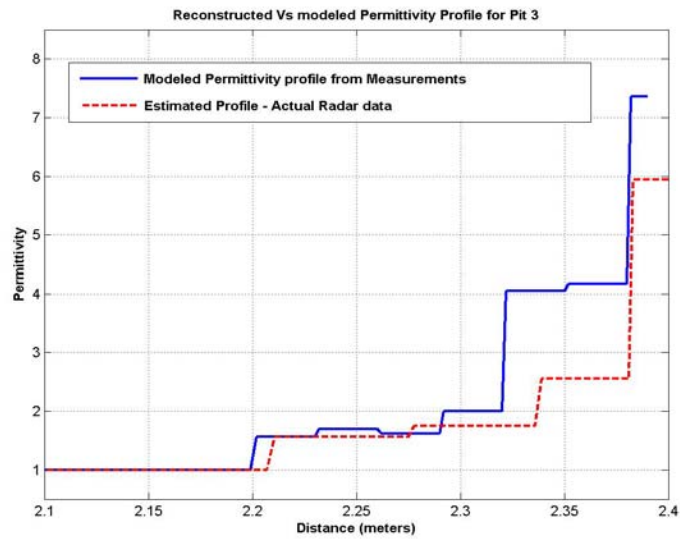
Figure 5-9 Reconstructed Vs modeled profile for Pit 3

5.2 Tests at the Sandbox lab at RSL

The inversion algorithm was also tested on data collected in the sandbox facility of the RSL lab at the University of Kansas. This facility consists of a rectangular box filled with quartz sand and is built with a system such that an antenna can be mounted to

be looking downwards (towards the sand). A network analyzer is used in place of a radar and is connected to the antennas using RF cables. The network analyzer is connected to a computer using a General Purpose Interface Bus (GPIB) card and can be controlled using MATLAB. A detailed description of the sandbox set-up and the RF circuitry is given in Chapter 5 of [25].

The operating parameters such as start frequency, bandwidth, number of samples and sweep time are set in the network analyzer, and calibration is performed at the input to the antennas. To remove system effects, a flat aluminum plate is laid over the sand surface and S_{11} measurements are taken. Then the targets are buried under sand and the S_{11} is measured over the frequencies of interest. Typically, the mismatch between the cable and the antenna is very large, and its sidelobes can mask small reflections buried under sand. This mismatch is removed by performing a Sky test where the antenna is pointed upward in such a way that there is no reflecting surface at least within the maximum unambiguous range of the system. The Sky test measurements are then subtracted from the actual measurements and the Fourier transform of this signal yields the range profile.

The inversion algorithm was tested on data collected using an HP 8753D network analyzer. The network analyzer parameters are tabulated in Table 5-4 below. A TEM horn antenna (operating in the 2-18 GHz frequency range) was used to take measurements. A bandwidth of 5 GHz was chosen so that we could have a resolution of 3 cm. Such a fine resolution is desired so that we could stack up layers (wood, Styrofoam) of small thickness in such a way that the measurements could be taken without altering the antenna arrangements in the sandbox.

Table 5-4 Network Analyzer Parameters for Sandbox experiment

Start Frequency	2 GHz
Stop Frequency	7 GHz
Number of frequency samples	1601
Sweep time	800 ms
Transmit Power	0 dBm
Calibration type	1 port
IF Bandwidth	3000 Hz
Antenna type	TEM Horn
Antenna Gain	10 dB

The network analyzer was set in the stepped frequency mode so that it is equivalent to a stepped-frequency radar. As described earlier, the network analyzer was interfaced with a computer and single port calibration was performed. Then, the sky shot measurements were taken. Figure 5-10 shows the target structure that was set up to test the inversion algorithm.
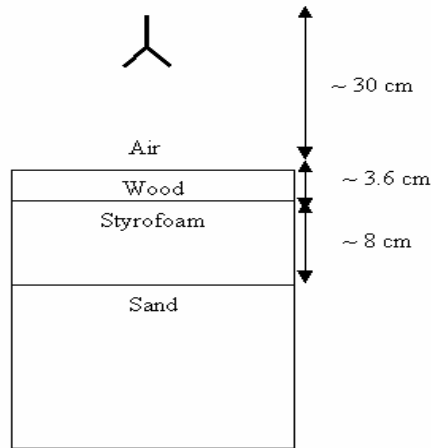
Figure 5-10 Multilayered Target stack to test inversion algorithm

It can be seen that there are four layers which form a dielectric stack giving rise to three interfaces. The residual mismatch between the antenna and the cable is removed by filtering and the filtered signal (in the linear scale) is shown in Figure 5-11.
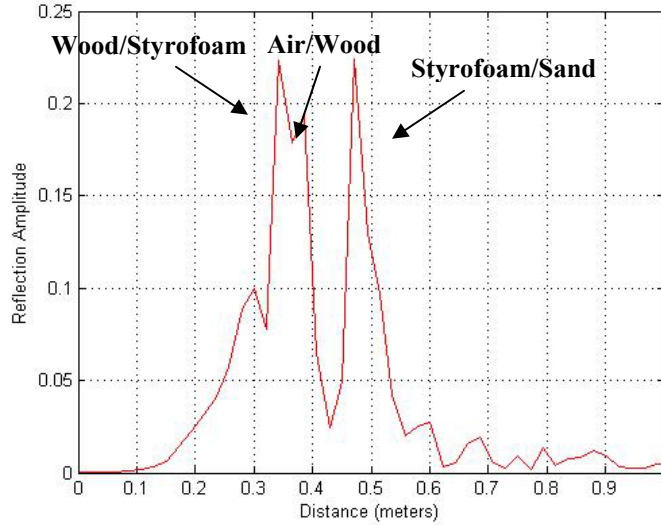
Figure 5-11 Stack return after calibration and filtering

Now, the MUSIC algorithm is applied on this signal to enhance the profile and estimate the time delays corresponding to signals. Figure 5-12 shows the enhanced range profile obtained using MUSIC.
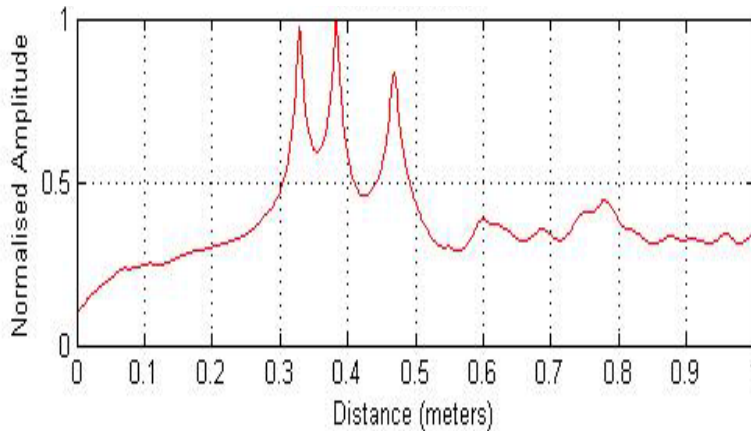
Figure 5-12 Range Profiles obtained using MUSIC for multilayered stack

Clearly, MUSIC is able to resolve the three major reflections as seen from Figure 5-19. However, the Maximum Likelihood MUSIC estimator could not correctly estimate the reflection coefficients. This could be due to the non-Gaussian nature of noise. For estimating the amplitudes, the layer stripping approach was used. The time delays

corresponding to valid reflections were obtained using MUSIC and the amplitudes were estimated using the recursive equations of Chapter 2. Figure 5-13 shows the reconstructed profile.
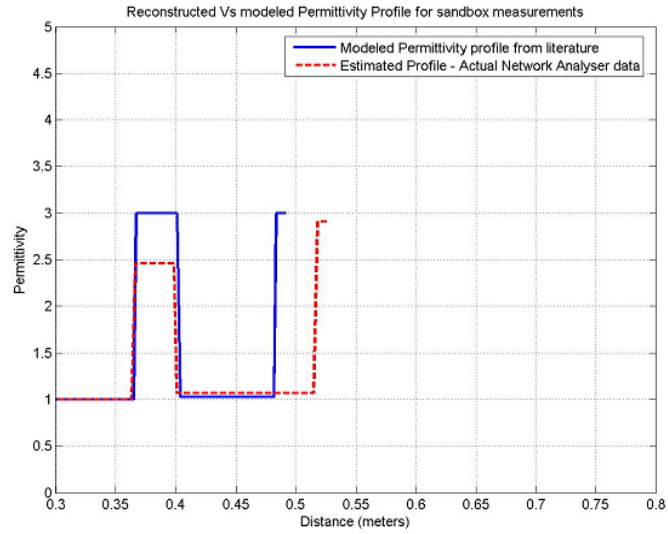
Figure 5-13 Reconstructed Vs actual Permittivity profile of multilayered stack

The reconstructed profile reasonably matches the true profile. For the second layer, the algorithm has predicted a value of 2.5. However, the true value of the permittivity of sand was not measured, and since a value between 2.5 and 3.5 has been documented [26], a value of 3 was chosen for modeling. Hence, the algorithm has yielded a reasonable estimate. We also observe a deviation in the position of the third interface (between Styrofoam and sand). This deviation can be attributed to the fact that a permittivity of 2 was chosen for velocity correction in order to identify the reflecting boundaries.

5.3 Experiments in Greenland

The Greenland sea-ice research team of the RSL used a prototype of a Plane Wave radar in Greenland during the summer 2004 season, with the objective of estimating the thickness of snow over sea-ice. We used this data as yet another test case for the inversion algorithm. Table 5-5 shows the specifications of the radar prototype.

Table 5-5 Network Analyzer Parameters for Plane Wave measurements in Greenland

Type of radar	Step Frequency
Start Frequency	12 GHz
Bandwidth	6 GHz
Sweep Time	4.72 sec
No. of frequency points	801

Radar measurements were taken over a horizontal traverse of 80 m, with ten measurements every 1 meter. Core data was also collected at three different pits close to the test site. Stratigraphy maps were observed at a couple of points along the grid. Figure 5-14 shows the relative positions of the core sampling areas with respect to the area where radar measurements were taken. It is clearly seen that Pit 2 is the only core reasonably close to any of the radar measurements and may provide a reasonable reference for radar measurement at the record marked 0. Hence, our objective was to invert the data at record 0 and compare the estimated permittivity profile with the core data and the stratigraphy map at record 0. Figure 5-15 shows the set-up of the plane wave experiment.
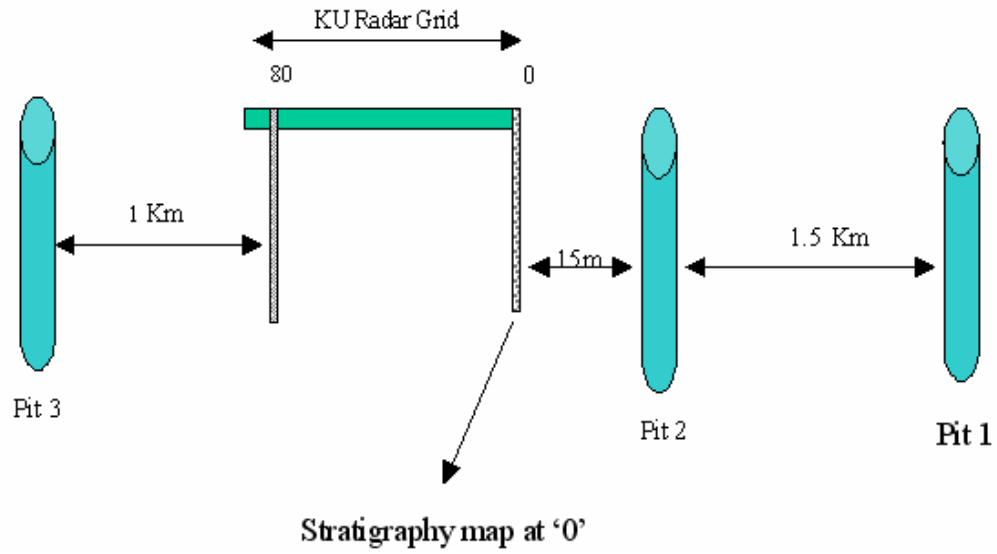
Figure 5-14 Relative locations of measurement grid and cores
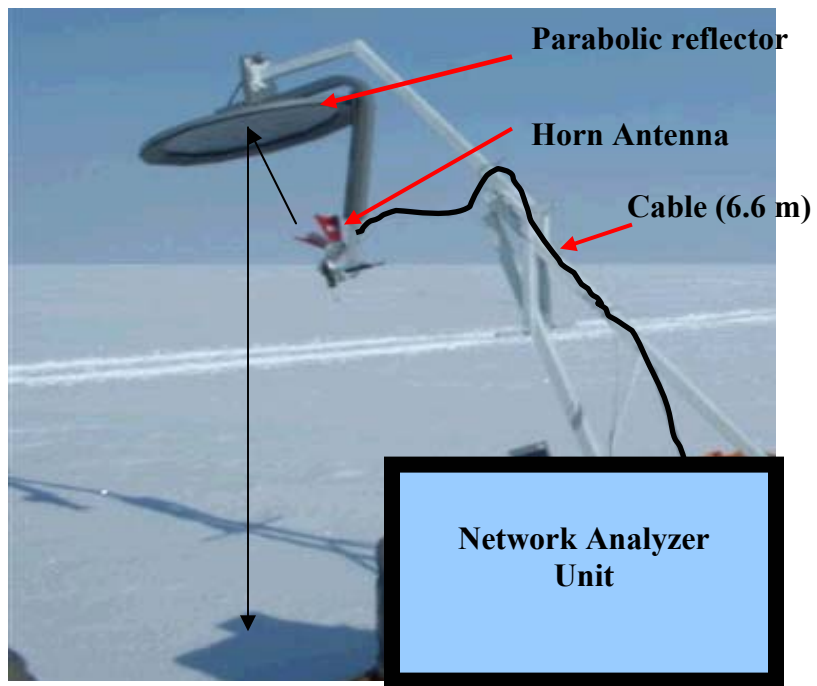
Figure 5-15 Experimental set up of the plane wave test

The network analyzer is connected to a horn antenna which then radiates the transmitted signal to the parabolic reflector. The EM wave radiated from the reflector is approximately a plane wave. The network analyzer is calibrated at its terminals and hence the observed distances are with respect to this terminal. The cable connecting the horn antenna to the analyzer measured around 6.6 meters and "loop" distance between the horn and the snow surface is around 3.1 meters.

Figure 5-16 shows the echogram of the measurements along the grid. It can be seen that the surface layer (marked as 1) occurs around a distance of 9.7 meters (6.6 meters of the cable plus a loop of 3.1 meters) followed by two discontinuous layers (marked as 2) at around 10.5 meters and 10.7 meters. The echogram also indicates the presence of a discontinuous layer at around 11.6 meters (marked as 3) . Layers 2 and 3 could be annual snow layers which get compressed, leading to higher densities.
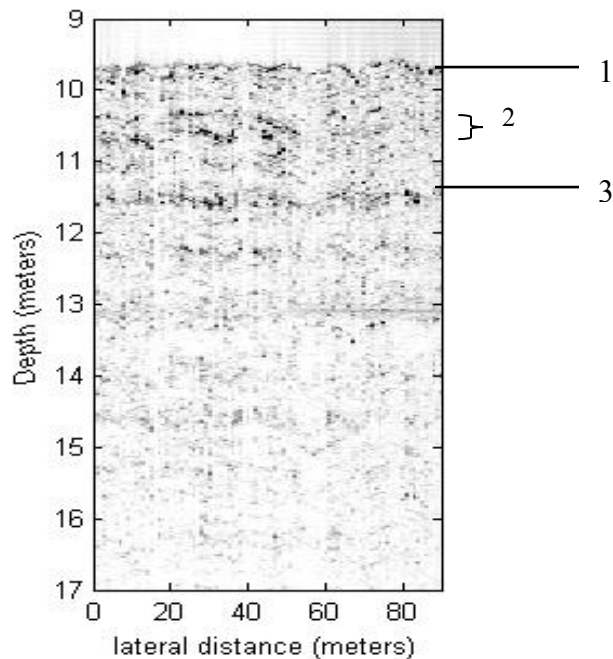
Figure 5-16 Echogram of radar measurements along the KU radar grid

Figure 5-17 shows the radar measurements at record 0 (after filtering any spurious signals). The peak at around 6.5 meters is due to the mismatch between the cable and the horn antenna. The surface return is observed at around 9.7 meters.
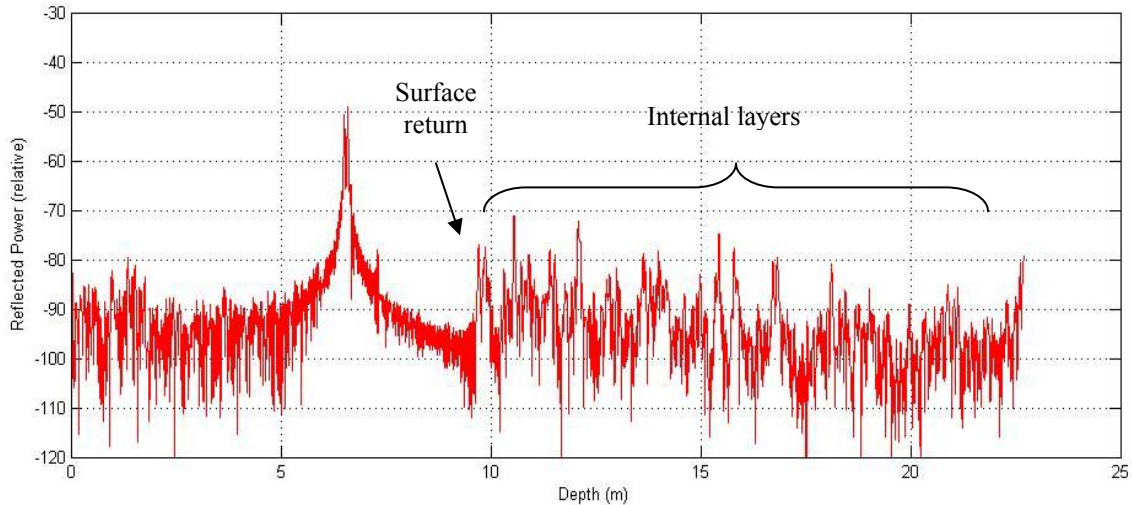
Figure 5-17 Radar measurement at record 0 (after subtracting the sky shot return)

Here, an interesting observation in the above figure is that several reflections corresponding to internal layers are higher than the surface return. Intuitively, it can be understood that inverting this profile directly would lead to abnormal values of permittivity (because of abnormal reflection amplitudes) and hence the observed data needs to be analyzed and any irregularities need to be removed.

These strong peaks could be due to any of several reasons: abrupt density changes, multiple reflections from internal snow layers, clutter due to scattering effects, system noise, or reflections from static objects like the antenna pole. Since the inversion algorithm works best on data free from system effects and clutter, it is necessary to eliminate these effects before applying the inversion algorithm on this data.

A good way to check for reflections from stationary targets is to compare adjacent records and look for similarity in the occurrences of peaks at the locations of interest. Applying the same test to our problem, we found no consistency in the appearance of the stronger reflections. Hence, we can conclude that these reflections are not from stationary targets. Next, we used the density data from the nearest snow pit (marked as Pit 2 in Figure 5-14) and modeled the permittivity profile using the dry snow permittivity model [9]. From this profile, we inferred that there is no drastic change in permittivity that could cause spikes to appear in the range profile. Using this permittivity profile, the range profile was modeled using Agilent's Advanced Design System (ADS) so that the effect of multiple reflections can be analyzed.
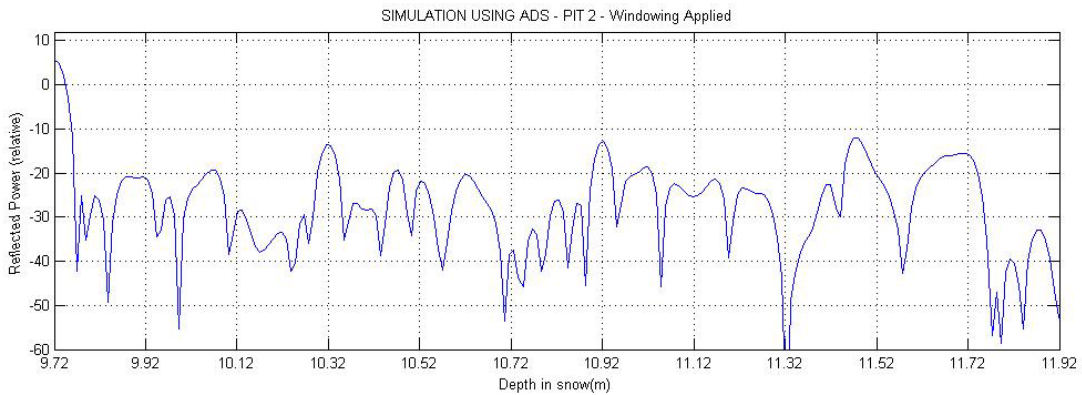
Figure 5-18 Simulated radar return of Pit 2 using ADS
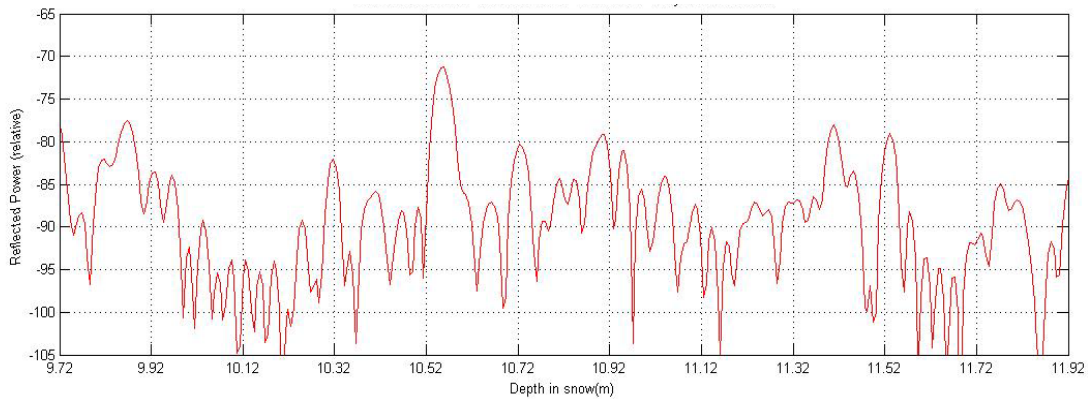
Figure 5-19 Actual radar return at record 0

Figure 5-18 shows a plot of the range profile modeled using ADS. This figure is compared with a profile of the observed return at record 0 (Figure 5-19). We find that there are several inconsistencies in the above comparison. Clearly, the ADS simulation shows that the surface return is dominant, whereas the actual data shows the presence of several strong returns either comparable to or greater than the surface return. Also, the positions of many of the peaks do not match well. Hence, we have insufficient information for this problem.

However, it was decided to test the inversion algorithm on data simulated using ADS. Figure 5-20 compares the range profiles obtained using FFT and MUSIC. Clearly, MUSIC is able to resolve internal reflections which appear embedded with the sidelobes of stronger returns. From this enhanced profile, delays corresponding to signal peaks were chosen and fed into the estimator, and the estimated permittivity profile is plotted in Figure 5-21.
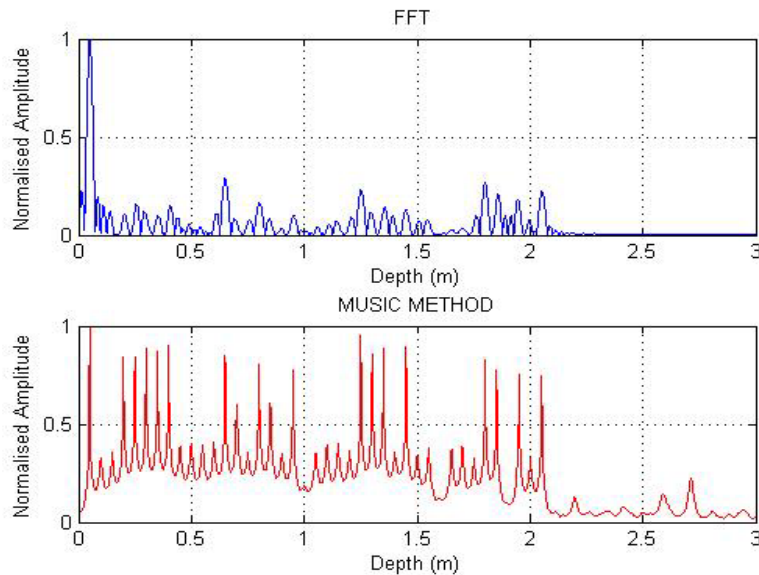
Figure 5-20 Range Profiles of simulated data obtained using FFT and MUSIC
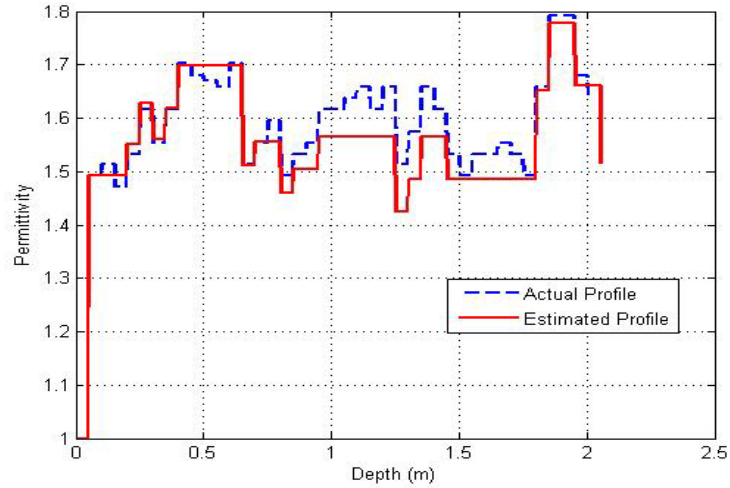
Figure 5-21 Reconstructed permittivity profile Vs actual (modeled) profile

In summary, the MUSIC-based inversion algorithm was successful in enhancing the profile in all three cases. But the amplitude estimator was only partly successful in inverse permittivity profiling due to the non-white/non-Gaussian nature of noise. However, in conjunction with the layer stripping method, we were able to successfully invert the data. The test on plane-wave data is still being researched, and with sufficient information about the internal layers of snow, the data can be inverted.

Chapter 6

GUI for the Inversion Algorithm

In order to make the enhancement and inversion algorithm accessible and easy to use, a Graphical User Interface (GUI) in MATLAB was developed. This chapter describes the features of the GUI and instructions for its use. Figure 6-1 shows a snapshot of the GUI. There are essentially three modules in this GUI .

6.1 Parameter declaration and File Selection:

The algorithm has been developed to work with the FMCW and the Step Frequency Radar, two of the commonly used radars in geological exploration. In the parameter declaration step, the user selects the type of radar data to work with. This is important since a unique forward model is required, depending on the type of radar. Once the user chooses the appropriate radar type, the GUI invokes the corresponding forward model into the algorithm.

The next step is to feed in radar data – which can be actual field data or data synthetically generated using empirical forward propagation models.

6.1.1 Actual radar data

In order to work with actual data, the recorded radar data file has to be stored in the user's local computer. The user can select any of the recorded data files and load the data into the GUI. It is important to note that this software can accept only a *.mat* file as input data. A few recorded radar data files taken by the RSL (which were tested using this GUI) can also be chosen by the user to get a better understanding of the algorithm. The type of radar used and the required radar parameters have been tabulated in Table 6-

1 for reference. The user can use any reasonable value for p from the eigen value chart. (The same column also shows a range of values which may be used).

Table 6-1 Reference radar parameters for the GUI

Radar data File	Type of radar	Band-Width (BW)	Start Freq (f_0)	Sweep time (Tp)	No. of freq. points	No. of reflections (from Eigen chart)
Antarctic dataset 1 Antarctic dataset 2 Antarctic dataset 3	FMCW	6 GHz	2 GHz	10 ms	-	20-40
RSL – GPR data	Step Frequency	7 GHz	2 GHz	800 ms	501	3-7
Greenland ADS data	Step Frequency	6 GHz	12 GHz	4.724 s	801	30-40

6.1.2 Synthetic radar data

The user may simulate radar data by using appropriate forward models. The inputs required here are the permittivities and corresponding depths (in meters) of each of the dielectric layers of the multi-layered profile. Also, the user enters the Signal to Noise Ratio (in dB) for the simulation. In this algorithm, we model noise as White Gaussian random process. The user can then view the fed-in permittivity profile.
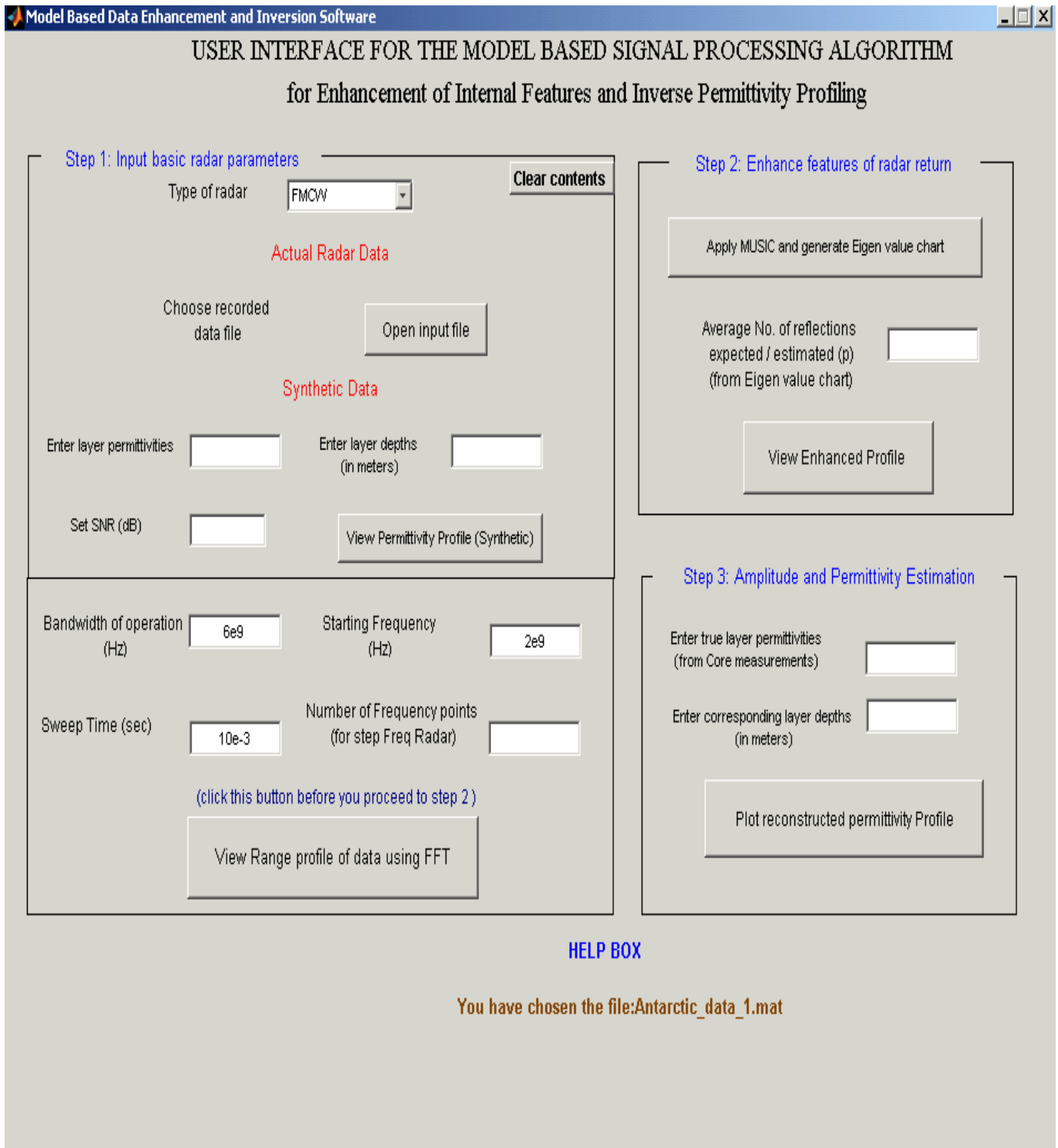
Figure 6-1 Snapshot of the GUI for model based data enhancement and inversion

The next step in the parameter declaration process is to feed in basic radar

parameters such as bandwidth of the radar (in Hz), starting frequency (in Hz) and sweep

time (in seconds). If a step frequency radar (or a network analyzer as in the case of RSL sandbox measurements) has been chosen, the user is required to enter the number of frequency points of the measurement. Once these parameters are entered, the range profile of the chosen data (using the conventional Fourier transform algorithm) can be viewed as a MATLAB figure. If an FMCW radar has been chosen, FFT gives the range profile, and if a step frequency radar has been chosen, the IFFT of the data gives the range profile of the data.

Note 1: It is assumed that the data fed in is calibrated and the antenna feed-through and other spurious signals have been filtered out.

Note 2: For an FMCW radar, the number of data samples has been fixed at 500. The rate at which the signal is sampled is a function of the maximum target depth and radar bandwidth and this in turn affects the number of samples (N) in the signal. This relationship is given by Equation 6.1, derived from [24].

$$\text{Max\_Depth} = \frac{F_b\ C\ T_p}{4\ B}\tag{6.1}$$

where C is the velocity of the EM wave, T_p is the sweep time, F_b is the beat frequency and B is the radar bandwidth. To process any depth profile, we may either change the number of data samples (N) or the radar bandwidth. But it was found that changing N was not a good solution, because the length of the signal influences the size of the autocorrelation matrix in MUSIC, and we found that large values of N frequently cause "Out of memory" problems in MATLAB, which terminate the GUI. Hence, it was decided to limit the number of samples to 500. However, this poses a condition on the bandwidth of the radar system entered by the user. Table 6.2 shows the maximum range

that can be processed for a given bandwidth. If the user enters a geo-profile such that the bandwidth does not support the maximum range, a warning message appears in the GUI asking the user to relax the bandwidth. *Please note that this applies only for FMCW radar simulation.* In the case of actual data, the user may resample the radar data such that the bandwidth-range relationship is satisfied (as was done for experimental Antarctic data).

Table 6-2 Bandwidth Vs range for N = 500

Bandwidth	Maximum range
6 GHz	3.12 m
5 GHz	3.75 m
3 GHz	6.25 m
1 GHz	18.7 m
0.5 GHz	37. 5 m

6.2 Enhancement of features

In this step, the radar data is enhanced by applying MUSIC algorithm. The number of frequency samples for spectral analysis is set at 16384 (2^{14}). This parameter is not critical, and is chosen to yield a finer spectrum. Following this, the user pushes the button intended to generate the eigen value distribution chart and enter the number of sinusoidal components expected in the actual signal. The amount of time taken to generate this graph can typically vary between a few seconds (for a small number of signal samples) to five minutes (for a large number of signal samples). Typically, the number of most significant eigen values (from the chart) is taken as the number of sinusoids in the signal. Once this value is fed in, pushing the *"View Enhanced Profile"* button generates two high-resolution enhanced spectral plots using MUSIC plotted against the frequency spectrum obtained by using the FFT – one with the distance axis

and the other with the time delay axis. As mentioned in Chapter 4, a good guess on the number of sinusoids yields a smoother profile. If the user chooses to enhance the profile with a different guess on the number of sinusoids, it is necessary to go back to the "Eigen value chart generation" step and then re-enter a new guess value. Reference values (of number of sinusoids) for the available radar data files can be seen in column 7 of Table 6.1.

6.3 Permittivity Estimation

In this step, the amplitude of the sinusoids is estimated using the amplitude estimation module discussed in Chapter 4. The GUI automatically selects the time delays corresponding to sharp peaks in the spectrum by choosing a threshold of 0.5 (which was considered reasonable after testing the algorithm on a large number of data sets. This threshold may be readjusted if so desired. From the amplitudes, the permittivity profile is reconstructed by using the recursive forward modeling equations of Chapter 2. Finally, the GUI plots the estimated permittivity values with depth. For comparison, the user may feed in the layer permittivities and their corrresponding depth values (from core measurements or any other *a priori* source). It may be noted that, for the already available data sets and synthetic data, the true profiles need not be fed in — they have been pre-defined in the GUI.

If the user chooses to work with a new data set, he may do so by starting from step 1; however, the contents of the workspace need be cleared by clicking the *"Clear Contents"* button in the right-hand corner of step 1 of the GUI.

Note: For the GPR-sandbox test, inversion was performed using the layer stripping approach. The MUSIC amplitude estimator did not yield a reasonable estimate because of the non-Gaussian nature of noise.

6.4 Sample Demonstration

Here, we give a step-by-step illustration for working with the GUI for both synthetic and actual radar data.

6.4.1 Synthetic radar data

- Invoke the GUI from the MATLAB command prompt using this command :

```
>> cd D: \
>> MBSP (to start the GUI)
```

STEP 1

- Select the type of radar you wish to simulate.

- Enter layer permittivities, depths, and SNR, and click the *"View permittivity profile (Synthetic)"* button. (A few flag variables have been initialized in this step, so do not proceed without clicking this button.)

- Enter radar parameters - Bandwidth, starting frequency, sweep time and number of frequency points (this parameter is necessary only if you have chosen a step frequency radar).

- Do not proceed to step 2 before clicking the *"View range profile"* button. This is because several key parameters for data enhancement are defined upon clicking this button.

STEP 2

- Click the *"Apply MUSIC"* button to generate the Eigen value chart. This process can take several seconds/minutes depending upon the data length and the processing speed of the computer. The eigen value chart shows the distribution of eigen values.

- Estimate the number of strongest eigen values seen in the chart and feed in the value of *'p'* – the average number of sinusoids in the signal (expected).

- Clicking the "*View Enhanced Profile*" button plots two high-resolution MUSIC-enhanced profiles: a) with respect to time delay axis, and b) with respect to distance axis.

- At this point, if you choose to re-enhance the profile with a different *'p'* value, you need to go back to the first button in step 2 and generate the Eigen value chart.

STEP 3

- Since this is simulated data, you need not re-enter the true layer permittivities/layer depths. These values will be taken from the values already entered in step 1.

- Click the "*Plot reconstructed permittivity profile*" button to estimate the permittivity profile and to plot it against the true profile.

- If you wish to work with a different data set/different radar type, click the "*Clear contents*" button on the right-hand corner of step 1.

6.4.2 Actual radar data

- Invoke the GUI from the MATLAB command prompt using this command

>> cd D: \
>> MBSP (to start the GUI)

STEP 1

- Select the type of radar you wish to simulate.

- Push the "*Open input file*" button to select the recorded radar data into the GUI. This data can be either your own radar data file or any of the recorded RSL data files (which were tested using this algorithm).

- Enter radar parameters - Bandwidth, starting frequency, sweep time and number of frequency points (this parameter is necessary only if you have chosen a step frequency radar). It is very important that the type of radar and the corresponding radar data match. Please refer to Table 6.1 for working with RSL data.

STEP 2

- Push the "*Apply MUSIC*" button to generate the Eigen value chart. This process can take several seconds/minutes depending upon the data length and the processing speed of the computer. The Eigen value chart shows the distribution of Eigen values.

- Estimate the number of strongest Eigen values seen in the chart and feed in the value of '*p*' – the average number of sinusoids in the signal (expected).

- Clicking the "*View Enhanced Profile*" button plots two high-resolution MUSIC-enhanced profiles: a) with respect to time delay axis, and b) with respect to distance axis.

- At this point, if you choose to re-enhance the profile with a different '*p*' value, you need to go to back to the first button in step 2 and generate the Eigen value chart.

STEP 3

- If you have chosen any of the RSL radar files, you need not re-enter the true layer permittivities/layer depths. These values have been pre-defined.

- Click the "*Plot reconstructed permittivity profile*" button to estimate the permittivity profile and to plot it against the true profile.

- If you wish to work with a different data set/ different radar type, click the "*Clear contents*" button on the right-hand corner of step 1.

Note: If you wish to access the source file for this GUI, at the MATLAB command prompt, enter " >> guide MBSP ".

Chapter 7

Summary and Future Work

7.1 Summary

Ground penetrating radars are being used to characterize features of the surface and the sub-surface. However, the GPR data are corrupted with noise, scattering, and losses due to the random nature of the underlying subsurface. In order to enhance the GPR return and then to estimate the underlying permittivity profile, a model-based algorithm was implemented and tested.

Algorithms based on MMSE minimization (Gauss-Newton) and spectral estimation (MUSIC) were developed (Chapter 3) and first tested on synthetic data in Chapter 4. It was found that the MUSIC algorithm – a spectral estimation technique – was more robust and is suitable for tests on actual radar data.

In Chapter 5, the MUSIC algorithm was applied on radar data collected during field experiments in Antarctica using an FMCW radar and on tests conducted at the sandbox facility at the RSL lab using a network analyzer. It was found that the MUSIC algorithm performed reasonably well to enhance the radar returns and to unmask the weak sidelobe embedded returns. The permittivity inversion part of the algorithm also performs well as long as the noise statistics are that of AWGN. In the sandbox test, MUSIC was only partly successful; however, in conjunction with the layer stripping method, we were able to successfully invert the data. Finally, a Graphical User Interface (GUI) for the model-based inversion algorithm was also developed in MATLAB.

7.2 Future Work

The accuracy of model-based techniques for data inversion depends on several factors – here are a few:

1. Accuracy of the mathematical model that represents the radar response

2. Accuracy of the measurement and calibration system

3. Signal to noise ratio of the system

4. Effects of clutter and scattering due to rough surface

Hence it is important that the mathematical model be thoroughly tested using several cases of synthetic data. Calibration errors can drastically change the amplitude and phase of the actual signal and hence, the calibration of the radar system must be undertaken with great care.

In this work, we have only considered the case of specular reflection and the effects of clutter; surface scattering and attenuation have been neglected from the model. Incorporating these effects into the model can enhance the performance of the inversion algorithm.

Inversion methods based on three-dimensional modeling, such as the Method of Moments (MOM) and Finite Difference Time Domain (FDTD), take into account the effects of scattering due to random surfaces and the three-dimensional antenna beam pattern; hence, they can be implemented for the forward model to yield better inversion results.

Appendix A

Modeling the complex dielectric constant of snow cover on sea ice

Snow can typically occur in two phases – dry and wet. Dry snow is a mixture of ice and air and does not contain water, whereas wet snow includes water. Table 5-2 shows that the Antarctic snow is a mixture of wet snow and brine.

To model the dielectric constant of this mixture, we first model the permittivity of wet snow using the empirical *Debye-like model* [9], where the real part of permittivity is mathematically modeled as:

$$\varepsilon'_{ws} = A + \frac{B \; m_v^{\;x}}{1 + \left(\dfrac{f}{f_0}\right)^2} \tag{A.1}$$

and the imaginary part is modeled as

$$\varepsilon''_{ws} = \frac{c \left(\dfrac{f}{f_0}\right) m_v^{\;x}}{1 + \left(\dfrac{f}{f_0}\right)^2} \tag{A.2}$$

where $f_0 = 9.07 \; GHz$, the effective relaxation frequency of wet snow, m_v denotes the moisture content in volume percentage, c represents the free space velocity, f is the frequency variable and the constants A, B and x are derived from experimental data as given in [9]. Once the wet snow permittivity has been modeled, we then model the

permittivity of brine using the formulation developed by Stogryn [26]. The real and imaginary parts of the complex dielectric constant of brine are given as:

$$\varepsilon_b' = \varepsilon_{w\infty} + \frac{\varepsilon_{b0} - \varepsilon_{w\infty}}{1 + \left(2\pi f \tau_b\right)^2} \tag{A.3}$$

$$\varepsilon_b'' = \frac{2\pi f \tau_b \left(\varepsilon_{b0} - \varepsilon_{w\infty}\right)}{1 + \left(2\pi f \tau_b\right)^2} + \frac{\sigma_b}{2\pi\varepsilon_0 f} \tag{A.4}$$

where $\varepsilon_{w\infty}$ is a dimensionless quantity equal to the high frequency limit of the dielectric constant of pure water, ε_{b0} is the static dielectric constant of brine, σ_b, τ_b are the conductivity and relaxation time, respectively, of brine and are empirically related [9] to the normality and temperature of brine in the mixture.

Finally, we model the permittivity of the mixture by treating brine as an inclusion within a wet snow mixture and using the mixing formula as given in [27].

$$\Delta\varepsilon_{mix} = \frac{\chi V_b \left\{\varepsilon_b - \varepsilon_{ws}\right\}}{\left[1 + \left(\dfrac{\varepsilon_b}{\varepsilon_{ws}} - 1\right)A_0\right]} \tag{A.5}$$

From Equation 5.5, the effective permittivity of the mixture is calculated as

$$\varepsilon_{eff} = \varepsilon_{ws} + \Delta\varepsilon_{mix} \tag{A.6}$$

where $\varepsilon_{ws} = \varepsilon_{ws}' + j\varepsilon_{ws}''$, the complex permittivity of wet snow, χ denotes the coupling factor considering brine inclusions to be isotropically oriented oblate

spheroids, A_0 is the depolarization factor, and V_b is the brine volume fraction which is a

function of the salinity and temperature of brine [9].

Evaluating the above expressions, the effective permittivities and their

corresponding distances are tabulated in Table A-1 below.

Table A-0-1 Modeled Permittivity Profile

Layer Thickness (m)	$\varepsilon_{effective}$ (Modeled - complex)	$\varepsilon_{effective}$ (Modeled - Absolute)
1.83	1.0000	1.00
0.03	1.45 + j 0.0193	1.44
0.03	1.60 + j 0.0175	1.60
0.03	1.70 + j 0.0021	1.70
0.03	1.77 + j 0.0044	1.77
0.03	1.74 + j 0.0016	1.74
0.03	1.71 + j 0.0029	1.71
0.03	1.64 + j 0.0104	1.65
0.03	1.66 + j 0.0121	1.66
0.03	1.66 + j 0.0462	1.67
0.03	1.71 + j 0.0576	1.71
0.03	1.70 + j 0.061	1.71
0.03	1.69 + j 0.0692	1.69
0.03	1.67 + j 0.0066	1.68
0.03	2.19 + j 0.1739	2.20
0.015	6.13 + j 1.2496	6.35
Ice bottom	3.14	3.14

References

[1] Mars Instrument Development Project (MIDP) Technical document, JPL, NASA, 2002.

[2] L.P. Peters, Jr., J. J. Daniels, and J. D. Young, "Ground penetrating radar as a subsurface environmental sensing tool," *Proceedings of the IEEE*, vol. 82, pp. 1802–1822, Dec. 1994.

[3] G. Picardi et al., "The Mars Advanced Radar for Subsurface and Ionosphere Sounding (MARSIS): concept and performance," *Proceedings of the IEEE International Geoscience and Remote Sensing Symposium*, Hamburg, Germany, pp. 2674-2677, 1999.

[4] Carl Leuschen, "Surface Penetrating Radar for Mars Exploration," PhD Dissertation, Department of Electrical Engineering and Computer Science, The University of Kansas, 2001.

[5] R. Togneri, "Estimation Theory for Engineers", Department of Electrical, Electronic and Computer Engineering, The University of Western Australia, 2001 [online]. Available at: http://www.ee.uwa.edu.au/~roberto/teach/Estimation_Theory.pdf

[6] Albert Tarantola, *Inverse Problem Theory*, Elsevier Press, New York, 1987.

[7] D.J.Daniels, "Ground Penetrating Radar - second edition", Chapter 11, IEEE Radar, Sonar, Navigation and Avionics Series 15, 2004.

[8] F.T. Ulaby, R.K. Moore, and A.K. Fung, *Microwave Remote Sensing Active and Passive*: Vol. 2 Radar Remote Sensing and Surface Scattering and Emission Theory, Artech House, 1982.

[9] F.T. Ulaby, R.K. Moore, and A.K. Fung, *Microwave Remote Sensing Active and Passive*: Vol.3 – From Theory to Applications, Artech House, 1982.

[10] Carl Leuschen, et.al, "Simulation and design of Ground-Penetrating radar for Mars Exploration", *Proceedings of the 2001 International Geoscience and Remote Sensing Symposium IGARSS '01*, Sydney, Australia, July 2001.

[11] Olaf Eisen, "On the nature, interpretation, and application of electromagnetic reactions in cold ice", *PhD Dissertation*, Electrical Engineering, The Alfred Wegener Institute for Polar and Marine Research, Germany, 2002.

[12] Kuok Wai Wong, "Development of a Prototype of a 2-8 GHz FMCW Radar for Snow Thickness Measurement on Sea Ice", Master's Thesis, Department of Electrical Engineering and Computer Science, The University of Kansas, 2004.

[13] Dimitris G. Manolakis, Vinay K. Ingle, Stephen M. Kogon, *Statistical and Adaptive Signal processing,* McGraw Hill, 2000.

[14] R. Schmidt, "Multiple emitter location and signal parameter estimation," *Proceedings of RADC Spectrum Estimation Workshop*, pp 243-258, 1979.

[15] Monson Hayes, *Statistical Digital Signal Processing and Modeling*, J.Wiley, 1996.

[16] G.A.F. Seber, C.J.Wild, *Nonlinear Regression*, J.Wiley, New York, 1989.

[17] Umberto Spagnolini, "Permittivity Measurements of Multilayered Media with Monostatic Pulse radar," *IEEE Transactions on. Geoscience and Remote Sensing*, Vol. 35, No.2, pp. 454–463, March 1997.

[18] S. Stergiopoulos, editor, *Advanced Signal Processing Handbook: Theory and implementation for radar, sonar & medical imaging Real-time systems*, Chapter 5, CRC Press, 2000.

[19] Steven M.Kay, *Fundamentals of Statistical Signal Processing,* Vol I – Estimation Theory, Prentice Hall, New Jersey, 1993.

[20] Ronald Gallant, *Nonlinear Statistical Models,* John Wiley & Sons, 1993.

[21] Petre Stoica, Hongbin Li, Jian Li, "Amplitude Estimation of Sinusoidal Signals; Survey, New Results, and an Application,"

[22] H. Yamada, et.al., "Super resolution techniques for time-domain measurements with a network analyzer *," IEEE Transactions on Antennas and Propagation*, Vol. 39, No.2, February 91, pp. 454-462.

[23] Bin Chen, Philipos C. Loizou, "Frequency Estimation Based on a Projection – Matrix Decomposition," Journal/Conference information unavailable.

[24] Sudarsan Krishnan, "Modeling and Simulation Analysis of a FMCW Radar for Measuring snow Thickness," Master's Thesis, Department of Electrical Engineering and Computer Science, the University of Kansas, 2004.

[25] John Paden, "Bistatic/Monostatic Synthetic Aperture Radar for Ice Sheet Measurements," Master's Thesis, Department of Electrical Engineering and Computer Science, The University of Kansas, 2003.

[26] Available at:

http://zhangzc.jahee.com/chemcai/Dielectric%20Constant%20Table.htm#SECTION-S